THEORETICAL AND EXPERIMENTAL STUDY OF WIDE-BAND QUASI-PLANAR CONICAL ANTENNAS

by

TSUNGYIN WU

Presented to the Faculty of the Graduate School of
The University of Texas at Arlington in Partial Fulfillment
of the Requirements
for the Degree of

MASTER OF SCIENCE IN ELECTRICAL ENGINEERING

THE UNIVERSITY OF TEXAS AT ARLINGTON
AUGUST 2008

ACKNOWLEDGEMENTS

I would like to acknowledge my grandparents, parents, sister, and close relatives and friends for their support and encouragement. I would want to thank my supervising professor Dr. M. Lu for his patience and guidance. Also, I would like to acknowledge Dr. S. Tjuatja, Dr. J. Bredow, and B. Svihel for their help and support in my studies in the University of Texas at Arlington. This work is supported in parts by NSF grant ECS-0528964

July 18, 2008

ABSTRACT

THEORETICAL AND EXPERIMENTAL STUDY OF

WIDE-BAND QUASI-PLANAR

CONICAL ANTENNAS

Tsungyin Wu, M.S.

The University of Texas at Arlington, 2008

Supervising Professor: Mingyu Lu

Conical antennas are widely used in many applications because of their broad input impedance bandwidth and omni-directional radiation pattern. However, conical antennas usually have three-dimensional structures and are, hence, relatively difficult to fabricate and integrate. In this thesis, a quasi-planar conical antenna is designed, where dielectric loading mechanically stabilizes the antenna while maintaining the input impedance invariant within a broad band. Specifically, a few configurations of the quasi-planar conical antenna are simulated, fabricated, and tested. Simulation and measurement results show excellent agreements. It is concluded in this thesis that, the quasi-planar conical antenna is mechanically light and robust, easy to fabricate and re-configure, and it exhibits all of the nice electrical properties of conventional conical antennas.

TABLE OF CONTENTS

ACKNOWLEDGEMENTS……. iii

ABSTRACT……. iv

LIST OF ILLUSTRATIONS…….. vii

LIST OF TABLES……... xi

Chapter Page

1. INTRODUCTION…….. 1

2. ANTENNA DESIGN…… 8

2.1 Theory on Biconical Antenna…….. 11

2.2 Cone Shape Cavity Conical Antenna ……. 15

2.3 Cylinder-Cone Shape and Bended Ground Plane …….. 18

3. SIMULATION, FABRICATION AND MEASUREMENT…….. 20

3.1 Simulation……20

3.2 Fabrication…….. 21

3.3 Measurement……..24

4. RESULTS……... 27

4.1 Simulated VSWR Results…….. 27

4.2 Measured VSWR Results……37

4.3 Measured and Simulated Radiation Pattern ……38

4.4 Effect of Dielectric Material Length…… 42

4.5 Comparison Between Conical and Biconical Antennas…….. 46

5. SENSOR NETWORK LOCALIZATION ……. 54

5.1 Distance Estimation ……..54

5.2 Localization..... 58

REFERENCES..... 62

BIOGRAPHICAL INFORMATION..... 65

LIST OF ILLUSTRATIONS

Figure		Page
1.1	Wireless sensor network……	1
1.2	Lodge's biconical antenna proposed in 1898……	3
1.3	Carter's biconical antenna and conical monopole design in 1939……..	3
1.4	Schelkunoff's spherical dipole developed in 1940……..	4
1.5	Katzin's rectangular horn antenna in 1946……..	4
1.6	Master's diamond (triangular) dipole in 1947……..	4
1.7	Brillouin's omni-directional coaxial horn antenna in 1948……	5
1.8	Marie's wide-band slot antenna in 1962……5	
1.9	Harmuth's large current radiator in 1985…….. 5	
1.10	Oblique shape biconical antenna proposed in [18]…… 6	
1.11	Different shapes of conical antennas that are studied in [19]……6	
1.12	Configuration of the proposed antenna in [20]…….... 7	
1.13	Configuration of the planar UWB antenna proposed in [22]. (a) top layer (b) bottom layer…….. 8	
1.14	The proposed and fabricated dielectric loaded conical antenna in [28]….. 9	
1.15	The proposed quasi-planar conical antenna…… 10	
2.1	Biconical antenna geometry……11	
2.2	Biconical antenna radiated spherical waves…… 11	
2.3	Biconical antenna electric and magnetic fields, and associated voltage and current…….. 12	
2.4	Biconical antenna and conical antenna (monopole)…….. 15	
2.5	(a) The quasi-planar conical monopole antenna with cone shape cavity. (b) The cross-section cut view of the point A to A' in (a)……... 16	
2.6	Three configurations of the designed quasi-planar conical antennas……..18	

3.1 Illustration of a revolutionary object with respect to the vertical axis in the middle. (a) antenna geometry, (b) exterior equivalence, and (c) Interior equivalence……21

3.2 Cone shape cavity quasi-planar conical antenna……22

3.3 Cylinder-cone shape cavity quasi-planar conical antenna……23

3.4 Cylinder-cone shape cavity quasi-planar conical antenna with bended ground plane……23

3.5 HP810 Network Analyzer……24

3.6 Probe antenna used in the measurement……25

3.7 Antenna measurement setup……25

4.1 Dimensions of the cone shape cavity conical antenna……27

4.2 VSWR of cone shape cavity conical antenna shown in Figure 4.1……28

4.3 VSWR of cone shape cavity conical antenna shown in Figure 4.1 with narrower ε_r range……29

4.4 VSWR of cone shape cavity conical antenna shown in Figure 4.1 with the half-cone angle fixed at the ε_r=1.3 case (42.3 degree). ε_r is changed from 1.3 to 1.8……30

4.5 VSWR of cone shape cavity conical antenna shown in Figure 4.1 with the half-cone angle fixed at the ε_r=1.8 case (36.2 degree). ε_r is changed from 1.3 to 1.8……30

4.6 Dimensions of the cylinder-cone shape cavity conical antenna……31

4.7 VSWR of cylinder-cone shape cavity conical antenna shown in Figure 4.6. ε_r changes from 1.3, 1.5, 1.8, to 2.0, and ψ is 42.3, 39.6, 36.2, and 34.2 degree, respectively……32

4.8 VSWR of cylinder-cone shape cavity conical antenna shown in Figure 4.6 with the half-cone angle fixed at the ε_r=1.3 case (42.3 degree). ε_r is changed from 1.3 to 1.8……32

4.9 Dimensions of the cylinder-cone shape cavity conical antenna with bended ground plane……33

4.10 VSWR of cylinder-cone shape cavity conical antenna with bended ground plane. shown in Figure 4.9. ε_r changes from 1.3, 1.5, 1.8, to 2.0, and ψ is 42.3, 39.6, 36.2, and 34.2 degree, respectively……34

4.11 VSWR of cylinder-cone shape cavity conical antenna with bended ground plane shown in Figure 4.9 with the half-cone angle fixed at the ε_r=1.3 case (42.3 degree). ε_r is changed from 1.3 to 1.8…….. 35

4.12 Comparison of three types of the designed antenna simulated to 18GHz with ε_r=1.8 for the cone case, and ε_r=1.3 for the other two cases…….. 36

4.13 Measured VSWR of cone shape cavity conical antenna and comparison with simulated result. The left figure shows the dimensions of the fabricated antenna…….37

4.14 Measured VSWR of cylinder-cone shape cavity conical antenna and comparison with simulated result. The left figure shows the dimensions of the fabricated antenna…….37

4.15 Measured VSWR of cylinder-cone shape cavity conical antenna with bended ground plane and comparison with simulated result. The left figure shows the dimensions of the fabricated antenna…….. 38

4.16 Radiation pattern of cone shape cavity conical antenna at (a) 2GHz, (b) 5GHz, (c) 8GHz, (d) 11GHz, (e) 14GHz, and (f) 18GHz. Unit: dBi…… 39

4.17 Radiation pattern of cylinder-cone shape cavity conical antenna at (a) 2GHz, (b) 5GHz, (c) 8GHz, (d) 11GHz, (e) 14GHz, and (f) 18GHz. Unit: dBi…….. 40

4.18 Radiation pattern of cylinder-cone shape cavity conical antenna with bended ground plane at (a) 2GHz, (b) 5GHz, (c) 8GHz, (d) 11GHz, (e) 14GHz, and (f) 18GHz. Unit: dBi……41

4.19 Dimensions of the cone shape cavity conical antenna with ground plane length 0.06m……...42

4.20 Dimensions of the cone shape cavity conical antenna with ground plane length 0.18m……...43

4.21 Comparison of the VSWR of the four cases up to 6GHz…….. 43

4.22 Comparison of the VSWR of the four cases up to 18GHz……44

4.23 Comparison of the radiation pattern for four ground plane lengths at (a) 2GHz, (b) 5GHz, (c) 8GHz, (d) 11GHz, (e) 14GHz, and (f) 18GHz. Unit: dBi…….. 45

4.24 Dimensions of the cone shape cavity conical antenna. The half-cone angle ψ is 42.3 degree…….. 46

4.25 Dimensions of the cone shape cavity biconical antenna. The half-cone angle ψ is 63.7 degree…….. 47

4.26 Comparison of VSWR of the conical and biconical structure of the cone shape antenna when ε_r =1.3…….. 48

4.27 Comparison of radiation pattern of the cone shape conical and biconical antennas at (a) 2GHz, (b) 5GHz, (c) 8GHz, (d) 11GHz, (e) 14GHz, and (f) 18GHz. Unit: dBi…….…. 49

4.28 Dimensions of the cylinder-cone shape cavity conical antenna. The half-cone angle ψ is 42.3 degree…….…… 50

4.29 Dimensions of the cylinder-cone shape cavity biconical antenna. The half-cone angle ψ is 63.7 degree…….…… 51

4.30 Comparison of VSWR of the conical and biconical structure of the cylinder-cone shape antenna when ε_r =1.3……52

4.31 Comparison of radiation pattern of the cylinder-cone shape conical and biconical antennas at (a) 2GHz, (b) 5GHz, (c) 8GHz, (d) 11GHz, (e) 14GHz, and (f) 18GHz. Unit: dBi……..... 53

5.1 Sensor network setup and background measurement……...54

5.2 Time domain waveform of Figure 5.1 setup……55

5.3 Setup with a sphere target (17 inch away from the leftmost antenna)…….56

5.4 Time domain waveform for Figure 5.3…….. 56

5.5 Time domain waveform when the target is moved further to 21 inches….. 57

5.6 Setup for sensor network, the dimension is in centimeters for both axis… 58

5.7 Localization results for target location 1……59

5.8 Localization results for target location 2...…… 60

5.9 Localization results for target location 3……60

LIST OF TABLES

Table Page

5.1 Percent error of the distance measurements…….…….…….. 57

CHAPTER 1

INTRODUCTION

In recent years, wireless sensor network (WSN) has become more and more popular as it initiates revolutionary development of smart environment on many automation systems such as building, utilities industrial, home, shipboard, and transportation [1]. A WSN is first developed for military applications in battlefield surveillance, and it consists of spatially distributed autonomous devices using sensors to cooperatively monitor physical or environmental conditions [2]. Figure 1.1 shows an illustration of a wireless sensor network. Usually, it can be divided into two parts: data acquisition and data distribution, and they are monitored and controlled by a management center. Depending on the application, the system needs various components such as sensors, protocol, computing scheme, user interface, etc.

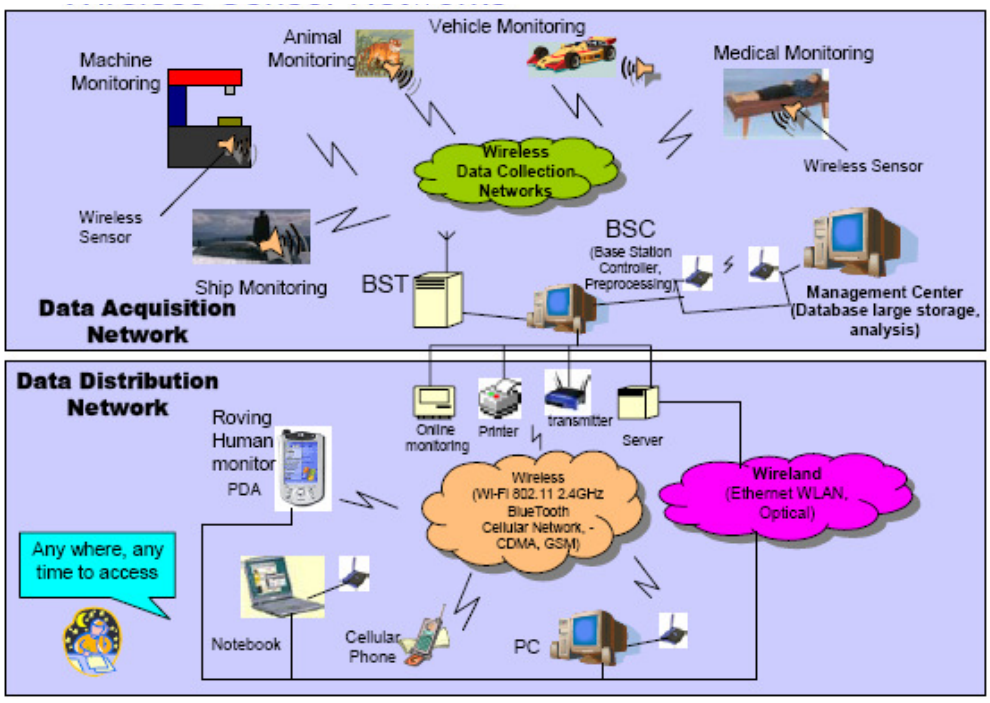

Figure 1.1: Wireless sensor network [1].

Antenna is one of the most important components in a WSN system. It is needed to perform wireless communications, and in many cases an antenna itself can be used as a sensor. The objective of this thesis is to develop an antenna for *Radar WSN*, in which the antenna fulfills two functionalities: communication and radar sensing [3]. Specifically, in the radar WSN, every wireless sensor node behaves as a radar: it transmits electromagnetic waves and detects echo waves to sense the surroundings. At the same time, wireless communication is necessary to collect data and coordinate the sensors. Here, we aim at developing one antenna as both the "radar antenna" and the "communication antenna." To achieve this goal, several requirements are imposed on the antenna design. First of all, it needs to be omni-directional for communicating and sensing along all azimuth directions, and it should also have certain elevation coverage. Secondly, it should be ultra-wideband (UWB), again, for both communication and sensing purposes. UWB allows for high data rate communication with low power consumption; and it enhances the sensing resolution (which is directly related to bandwidth) [4]. Moreover, the antenna is desired to be efficient, robust, small, light, cheap, and easy to fabricate and integrate.

The development of (UWB) antennas can be traced back to the early 1900s [5]. The word "Ultra-wideband" has its roots in the original "spark-gap" transmitters that pioneered radio technology [6]. In 1898, Oliver Lodge had a patent that disclosed spherical dipoles, square plate dipoles, biconical dipoles, and triangular dipoles. He also introduced the concept of a monopole antenna using the earth as a ground plane [7]. Figure 1.2 below shows the biconical configuration disclosed in Lodge's patent.

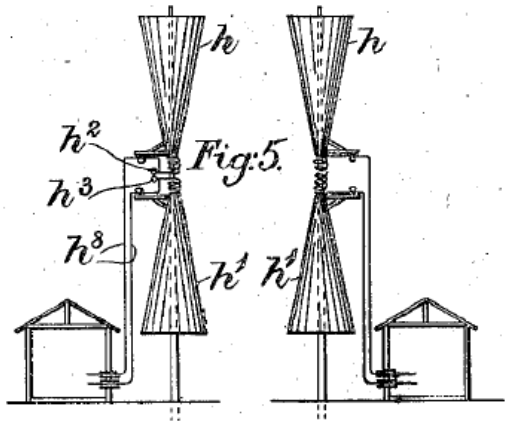

Figure 1.2: Lodge's biconical antenna proposed in 1898 [7].

However, as the frequency increases and wave becomes shorter, the economic advantages of a "thin wire" quarter antenna overcome any performances of Lodge's antenna. In 1930s, the invention of television and the need to transmit video signals lead to the rediscovery of the biconical antenna and conical monopole by Carter in 1939 [8].

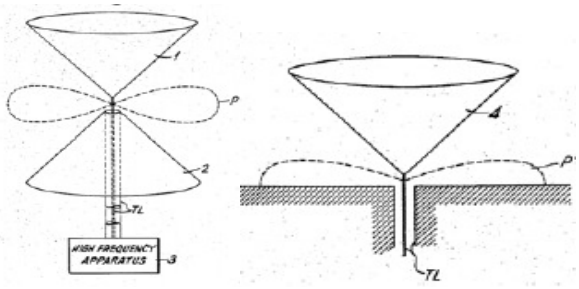

Figure 1.3: Carter's biconical antenna and conical monopole design in 1939 [8].

Carter improved upon Lodge's original design by incorporating a tapered feed [9]. Carter was among the first to take the key step of incorporating a broadband transition between feed lines and radiating elements.

Over the years, many other types of UWB antennas have been developed. Shown below are some of the key UWB antenna developments.

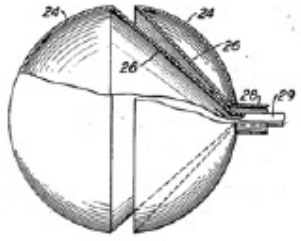

Figure 1.4: Schelkunoff's spherical dipole developed in 1940 [10][11].

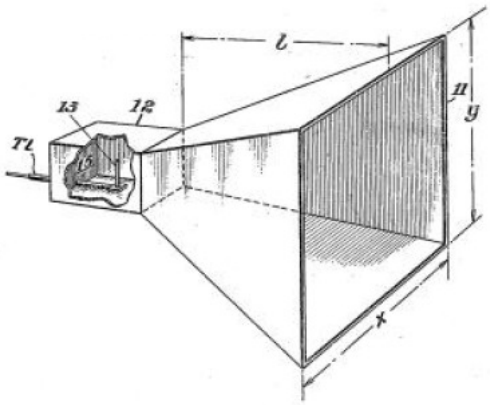

Figure 1.5: Katzin's rectangular horn antenna in 1946 [12].

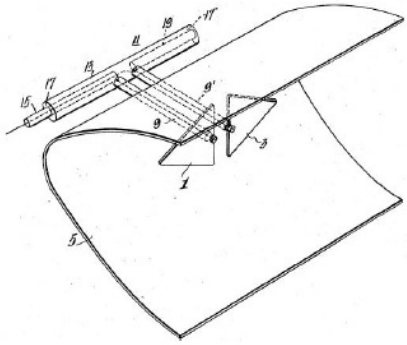

Figure 1.6: Master's diamond (triangular) dipole in 1947 [13].

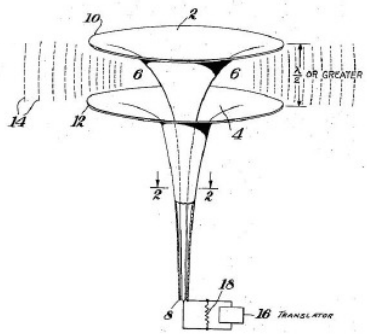

Figure 1.7: Brillouin's omni-directional coaxial horn antenna in 1948 [14].

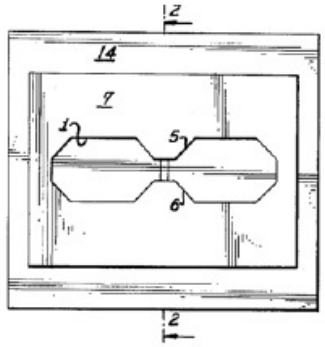

Figure 1.8: Marie's wide-band slot antenna in 1962 [15].

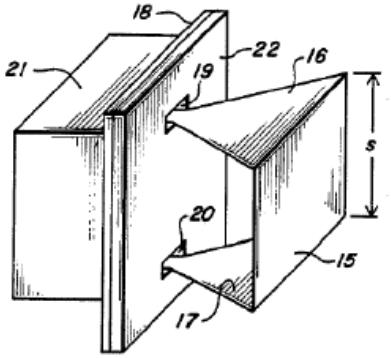

Figure 1.9: Harmuth's large current radiator in 1985 [16].

In a sensor network environment, as discuss above, the two basic properties that an antenna must have are wide-band and omni-directional characteristics. However, many types of the UWB antennas do not have omni-directional radiation. Even if they do, such as the one shown in Figure 1.7, the configuration is difficult to fabricate, and it does not look very robust. As

the result, the conical monopole antenna developed in 1939 (Figure 1.3) is the one that has both wide-band and omni-directional characteristics, and at the same time the configuration is the simplest amount these UWB antennas [17].

Many researches have been done to study both biconical and conical antennas. In [18], a biconical antenna with oblique edges is studied. Figure 1.10 shows the oblique shape biconical antenna in [18]. A mathematical expression is given to relate the shape to the radiated fields. By knowing this, we are able to tune the radiation direction.

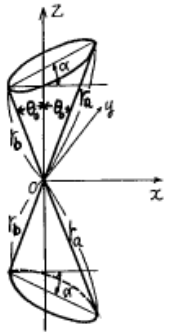

Figure 1.10: Oblique shape biconical antenna proposed in [18].

Figure 1.11 below shows some representative conical antenna shapes studied in [19]. In [19], it claims that if we consider the gain, the VSWR, and the volume of the antenna together, Figure 1.11(a) has the best performance amount all the shapes in Figure 1.11.

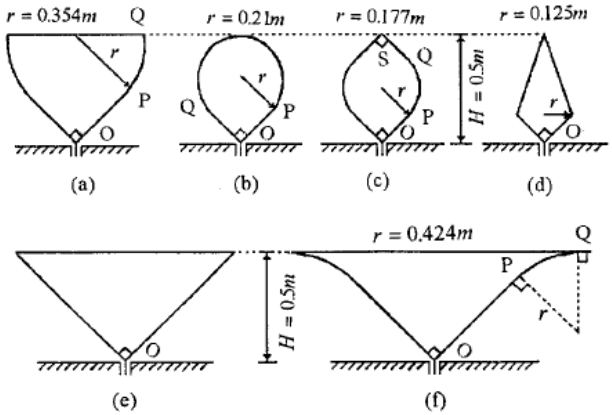

Figure 1.11: Different shapes of conical antennas that are studied in [19].

In [20], it is looking for an optimized conical antenna shape by adjusting the angles and lengths in Figure 1.12. The result of [20] comes out to be identical with [19]. In [20], it claims that Figure 1.11(a) is the optimal conical antenna shape that is broadband and low return loss.

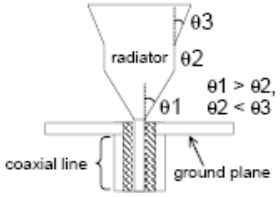

Figure 1.12: Configuration of the proposed antenna in [20].

However, all the above antennas are still not good enough in wireless sensor network applications. The major drawbacks are mechanical: having metal cones standing alone in the air is not easy to manipulate, fabricate, and maintain.

Quite a few methods have been proposed to improve the mechanical characteristics of conical antennas. In [21], thin wire structures are used to replace the cone surfaces. It is proven that most of the conical antenna performances remain the same when replacing the metal part with thin wire grids. However, it does not completely resolve the mechanical unreliability issue due to the fact that thin wires are still standing alone in the air, and it may be even more difficult to maintain.

Some researcher resorted to planar version of conical antennas, as in [22]. Figure below shows the proposed configuration. We can think of it as a printed circuit board version of the three-dimensional conical antenna. The results in [22] proof that the planar antenna keeps the wide-band omni-directional property that is similar to the conventional conical antenna.

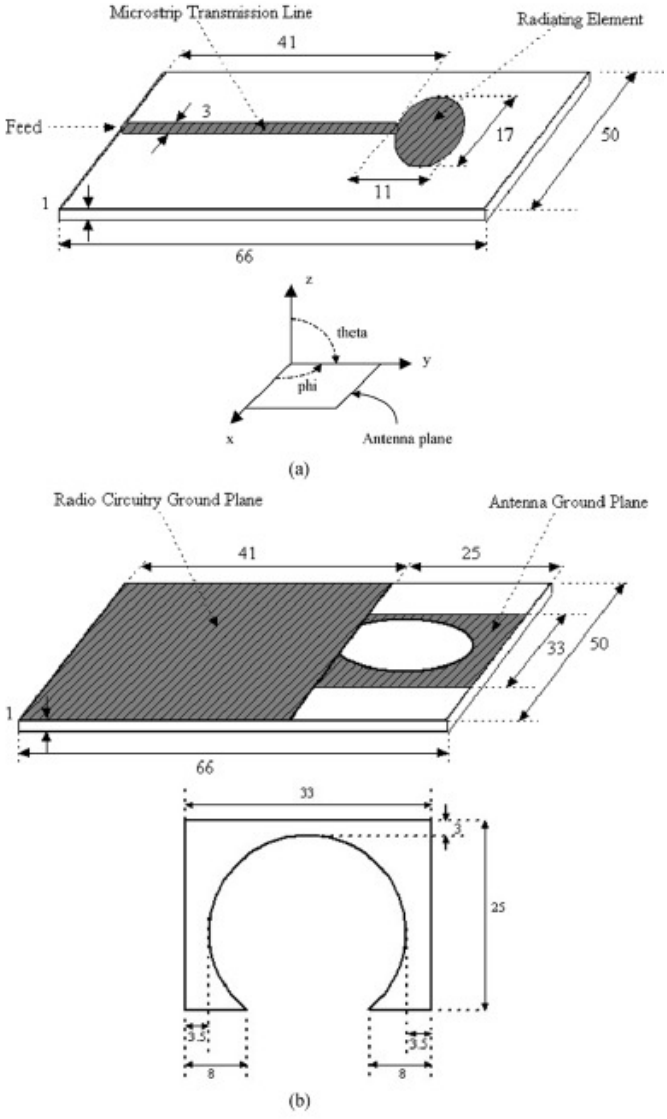

Figure 1.13: Configuration of the planar UWB antenna proposed in [22].
(a) top layer (b) bottom layer.

Many other studies are also focusing on broadband omni-directional planar antennas [23] [24] [25] [26] [27]. With slightly different shapes, they achieve broadband and omni-directional performances by a planar antenna. However, these planar antennas are still not perfect. Because of their omni-directional radiation, they must stand alone in the air to radiate

omni-directionally, and since they are planar, they can not stand alone without any help. In another word, they are not conformal.

A dielectric loaded conical antenna is reported in [28]. Figure 1.14 shows the proposed antenna in [28]. However in [28], the dielectric loading needs a special magnetic material, hence not practical. Also, the antenna is not really “broadband” (the claimed operating frequency range is 800-2500MHz).

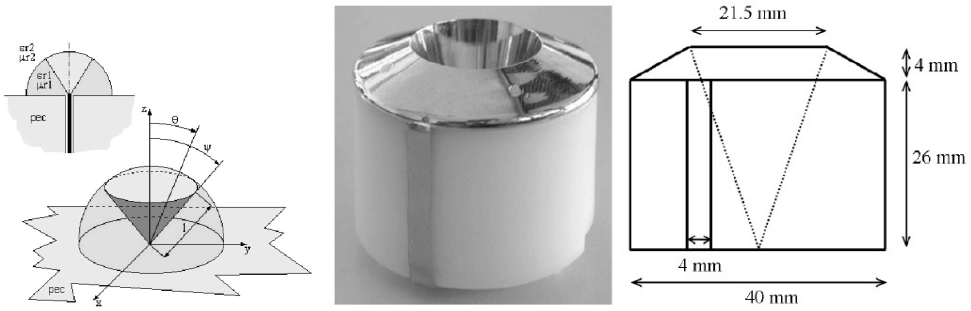

Figure 1.14: The proposed and fabricated dielectric loaded conical antenna in [28].

In this thesis, a quasi-planar conical antenna is proposed (Figure 1.15). A non-magnetic, light, and cheap dielectric supporting material is introduced to make the antenna mechanically reliable. At the same time, it keeps the wide-band and omni-directional performances of conventional conical antennas. It is easy to design, fabricate, and integrate. As shown in the quasi-planar monopole antenna in Figure 1.15, a cone-shaped cavity is etched on a piece of dielectric slab; a thin layer of metal is deposited onto the cavity wall to form the conical radiator; and a layer of metal at the bottom surface of the dielectric slab serves the ground plane. Comparing with the tradition conical antenna, it is robust and easy to re-configure. By saying robust, it means that the antenna is mechanical stable, and can last for a long time. By saying easy to re-configure, a design method is proposed, so that the antenna is easy to design base upon desired characteristics. Choice of dielectric loading material is the crucial in the design of quasi-planar conical antenna, and it will be explained in detail in Section 3.2. In this thesis, the quasi-planar conical antenna is simulated using a full-wave solver based on the Method of

Moments (MOM). Three types of antennas are fabricated and measured. Simulation and experimental results agree with each other very well; and they validate the wide-band omni-directional features of the designed antenna. Also in this thesis, the quasi-planar conical is applied to a simple radar WSN testbed to realize target localization.

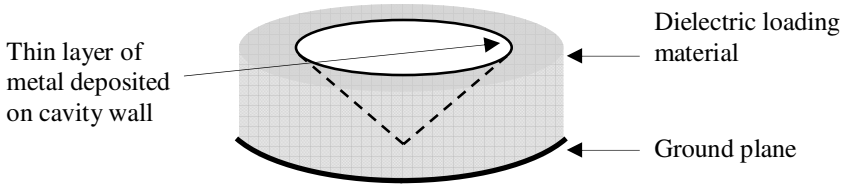

Figure 1.15: The proposed quasi-planar conical antenna.

In Chapter 2, the design procedures and considerations will be discussed. In Chapter 3, it talks about the simulation, fabrication, and measurement methods. Chapter 4 shows the results. In Chapter 5, a sensor network localization application using the proposed antenna is discussed.

CHAPTER 2

ANTENNA DESIGN

2.1 Theory on Biconical Antenna

Before designing the quasi-planar conical antenna, we have to first study the theory on the conventional conical antenna.

Figure 2.1 shows the well-known biconical antenna configuration. It is formed by two infinite large metal cones together. When applying a voltage between the two cone tips, it will produce outgoing spherical waves as shown in Figure 2.2.

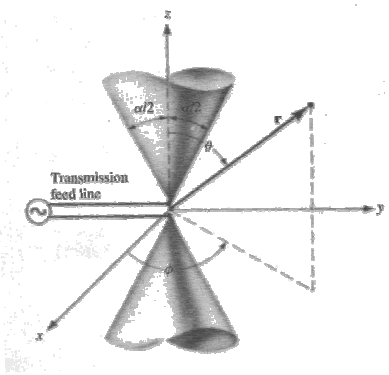

Figure 2.1: Biconical antenna geometry [29].

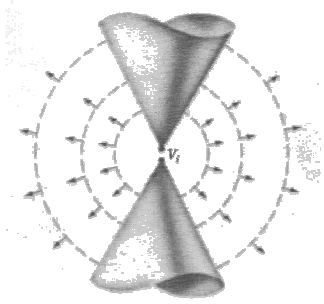

Figure 2.2: Biconical antenna radiated spherical waves [29].

2.1.1 Radiated Fields

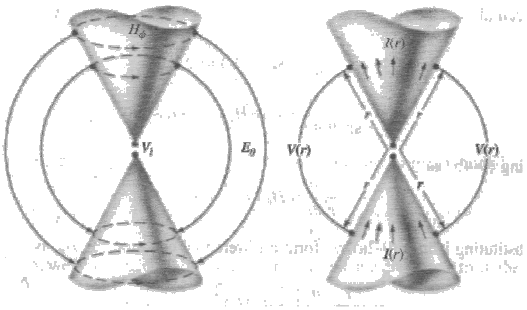

Figure 2.3: Biconical antenna electric and magnetic fields, and associated voltage and current [29].

In [29], the theoretical result of a biconical antenna is developed. Assume the excitation is TEM mode, so that electric and magnetic fields are transverse to the direction of propagation, as shown in Figure 2.3. By Faraday's Law, we can have:

$$\nabla \times \overline{E} = -j\omega\mu\overline{H} \tag{2-1}$$

In spherical coordinates, assume the E-field only has E_θ component, and it is independent of ϕ, the above equation can reduce to:

$$\nabla \times \overline{E} = \hat{a}_\phi \frac{1}{r}\frac{\partial}{\partial r}(rE_\theta) \tag{2-2}$$

Combine equation (2-1) and (2-2), we have:

$$\hat{a}_\phi \frac{1}{r}\frac{\partial}{\partial r}(rE_\theta) = -j\omega\mu\left(\hat{a}_r H_r + \hat{a}_\theta H_\theta + \hat{a}_\phi H_\phi\right) \tag{2-3}$$

Since the magnetic field only has H_ϕ component, the above equation becomes:

$$\frac{1}{r}\frac{\partial}{\partial r}(rE_\theta) = -j\omega\mu H_\phi \tag{2-4}$$

According to Ampere's Law:

$$\nabla \times \overline{H} = j\omega\varepsilon\overline{E} \tag{2-5}$$

Same as above, we expanded this into spherical coordinates, and we assume that only E_θ and H_ϕ exist, and they are independent of ϕ, we have:

$$\hat{a}_r \frac{1}{r^2 \sin\theta}\left[\frac{\partial}{\partial\theta}\left(r\sin\theta H_\phi\right)\right] - \hat{a}_\theta \frac{1}{r\sin\theta}\left[\frac{\partial}{\partial r}\left(r\sin\theta H_\phi\right)\right] = j\omega\varepsilon\left(\hat{a}_\theta E_\theta\right) \tag{2-6}$$

Since $\hat{a}_r$ component is zero, and the $\hat{a}_\theta$ should be equal, we have:

$$\frac{\partial}{\partial\theta}\left(r\sin\theta H_\phi\right) = 0 \tag{2-7}$$

$$\frac{1}{r\sin\theta}\left[\frac{\partial}{\partial r}\left(r\sin\theta H_\phi\right)\right] = -j\omega\varepsilon E_\theta \tag{2-8}$$

Equation (2-8) can be reduced to:

$$\frac{1}{r}\frac{\partial}{\partial r}\left(rH_\phi\right) = -j\omega\varepsilon E_\theta \tag{2-9}$$

Substitute equation (2-9) into (2-4), we can have:

$$\frac{\partial^2}{\partial r^2}\left(rH_\phi\right) = -\omega^2\mu\varepsilon\left(rH_\phi\right) = -k^2\left(rH_\phi\right) \tag{2-10}$$

A solution of equation (2-10) needs to also satisfy equation (2-7). For this reason, we can see that the solution must have the form:

$$H_\phi = \frac{f(r)}{\sin\theta} \tag{2-11}$$

One solution of (2-10) that also satisfies (2-11), which has outgoing traveling wave characteristic is:

$$H_\phi = \frac{H_0}{\sin\theta}\frac{e^{-jkr}}{r} \tag{2-12}$$

The inward traveling wave is also a solution, but in this infinitely long structure, it does not exist. Since the field is TEM mode excited, we can have the electric field expression:

$$E_\theta = \eta H_\phi = \eta \frac{H_0}{\sin\theta} \frac{e^{-jkr}}{r} \tag{2-13}$$

2.1.2 Voltage, Current and Input Impedance

Figure 2.3 above shows the voltage and current produced. By knowing E_θ and H_ϕ, we can calculate the voltage and current that has a distance r from the origin.

$$V(r) = \int_{\frac{\alpha}{2}}^{\pi-\frac{\alpha}{2}} \bar{E} \cdot d\bar{l} = \int_{\frac{\alpha}{2}}^{\pi-\frac{\alpha}{2}} \left(\hat{a}_\theta E_\theta \right) \cdot \left(\hat{a}_\theta r d\theta \right) = \int_{\frac{\alpha}{2}}^{\pi-\frac{\alpha}{2}} E_\theta r d\theta \tag{2-14}$$

where α is the cone angle shown in Figure 2.1.

We can further substitute equation (2-13) into (2-14), and have the voltage expression reduced to:

$$V(r) = 2\eta H_0 e^{-jkr} \ln\left[\cot\left(\frac{\alpha}{4} \right) \right] \tag{2-15}$$

The current on the surface of the cones, having a distance r from the origin is:

$$I(r) = \int_0^{2\pi} H_\phi r \sin\theta d\phi = H_0 e^{-jkr} \int_0^{2\pi} d\phi = 2\pi H_0 e^{-jkr} \tag{2-16}$$

Using the voltage and current, we can have the characteristic impedance written as:

$$Z_c = Z_{in} = \frac{V(r)}{I(r)} = \frac{\eta}{\pi} \ln\left[\cot\left(\frac{\alpha}{4} \right) \right] \tag{2-17}$$

We can see the characteristic impedance is not a function of the distance r. Therefore, this also represents the input impedance at the antenna feed point. The result shows the input impedance Z_{in} only depends on the cone angle α and the material intrinsic impedance η (in this case, $\eta = \eta_0$). Notice that Z_{in} does not depend on frequency. As a result, the input impedance of the biconical antenna is a constant throughout all frequencies.

2.2 Cone Shape Cavity Conical Antenna

Base on the biconical antenna theory, the goal is again to design an antenna with supporting materials and keep its original characteristics. However, before adding the dielectric loading, the problem can be simplified into a monopole antenna instead of a biconical antenna.

Figure 2.4 below shows the configuration of a monopole. Instead of two cones, one cone is replaced with an infinite metal plane conductor. In theory, their radiation properties are similar, and it shows that the input impedance of the monopole is one-half of the input impedance of the biconical antenna [29].

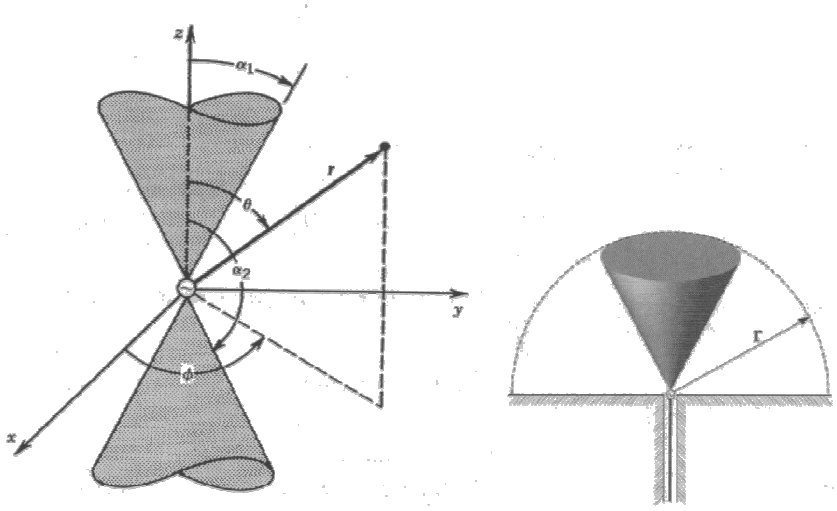

Figure 2.4: Biconical antenna and conical antenna (monopole) [29].

According to [30], a mathematical proof of the impedance is given. First, he derives the voltage and current for biconical configuration. Then, use

$$Z_c = \frac{V(r)}{I(r)} \tag{2-18}$$

it finally becomes,

$$Z_c = Z_{in} = \frac{\eta}{2\pi} \ln\left[\frac{\cot\left(\frac{\alpha_1}{2}\right)}{\cot\left(\frac{\alpha_2}{2}\right)}\right] \tag{2-19}$$

where α_1 and α_2 are the angles from the *z*-axis to the upper and lower cone. When $\alpha_2 = \pi - \alpha_1$, the equation 2-19 can be reduced to

$$Z_c = Z_{in} = \frac{\eta}{\pi} \ln\left[\cot\left(\frac{\alpha_1}{2}\right)\right], \tag{2-20}$$

and this is the biconical (symmetric) equation discussed earlier. When α_2 = 90 degree, the equation 2-19 can be reduced to

$$Z_c = Z_{in} = \frac{\eta}{2\pi} \ln\left[\cot\left(\frac{\alpha_1}{2}\right)\right], \tag{2-21}$$

and this is the conical case (the lower cone is replaced by a ground plane).

This gives a relationship of the impedances between conical and biconical antenna. As a result, we can transform a biconical antenna into a conical antenna, or vise vesa.

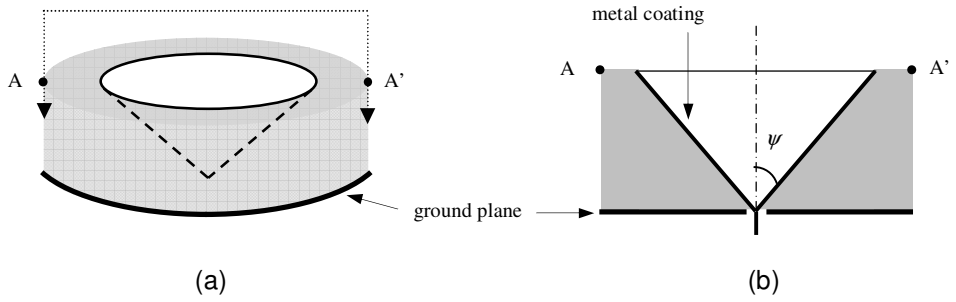

Figure 2.5: (a) The quasi-planar conical monopole antenna with cone shape cavity. (b) The cross-section cut view of the point A to A' in (a).

Now, base on the conical antenna shape, a dielectric material is added on the sides of the monopole as shown in Figure 2.5(a), and its cross section is shown in Figure 2.5(b). A cylindrical dielectric slab is made of material with permittivity $\varepsilon_r \varepsilon_0$ and permeability μ_0, where ε_0 and μ_0 are the permittivity and permeability of the free space, respectively. The bottom of the slab is coated by metal as the ground plane. A cone shape is etched in the slab, and metal is coated on the cone wall. The antenna is fed at the tip of the cone.

The input impedance equation of this material added antenna will be the same as the traditional monopole conical antenna, since the only difference is the material used. As we discuss earlier, the input impedance of this monopole antenna is:

$$Z_{in} = \frac{1}{2\pi}\sqrt{\frac{\mu_0}{\varepsilon_r \varepsilon_0}} \ln\left[\cot\left(\frac{\psi}{2}\right)\right] \tag{2-22}$$

where ψ is one-half of the cone angle shown in Figure 2.5(b). When transverse electromagnetic wave is fed to the tip of the cone, this antenna can be considered constituting a finite transmission line with the impedance mention above. To maintain constant input impedance, it all depends on the material property ε_r. If the material property ε_r stays constant over a range of frequencies, the input impedance will also maintain constant at the same range of frequencies. However, this is not an easy task. A dielectric material's electrical properties usually vary with respect to frequency. Specifically, the dielectric constant ε_r depends on frequency for most of the materials.

Secondly, when the transverse electromagnetic wave hits the end of the cone, it is reflected and scattered. As the operating frequency increases, the reflection and scattering decrease, and the antenna is behaving more and more like an infinitely long transmission line. The dielectric loading makes the wave's behavior more complicated. The dielectric material forms a cavity, similar to the cavity underneath a microstrip patch antenna. This cavity tends to store energy, hence would reduce the antenna's bandwidth. On the other hand, the wavelength within the dielectric material is shorter than that in the free space. As a result, the electrical length of the transmission line is enlarged due to the dielectric loading. Such variations may deteriorate the antenna's wide band feature if not carefully taken into account. Therefore, it is not easy to predict the effect of dielectric loading in a straightforward manner. To analyze the dielectric loaded conical antenna, a full wave simulation is carried out (further discuss in Chapter 3).

2.3 Cylinder-Cone Shape and Bended Ground Plane

To claim that the quasi-planar antenna is easy to manipulate, two more antennas are designed to compare the results. Figure 2.6 shows the further designs to improve the antenna performances.

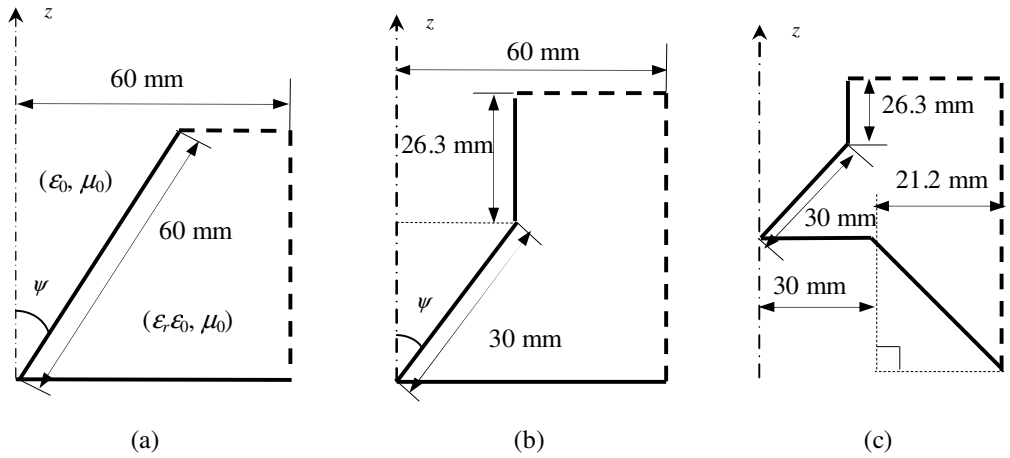

Figure 2.6: Three configurations of the designed quasi-planar conical antennas. (a) regular cone, (b) deformed cone, and (c) deformed dipole.

Due to revolutionary symmetry, geometries in *x-z* plane are sufficient to represent the antenna configuration. The solid lines stand for metal; and the dashed lines represent interfaces between the dielectric material and air. Figure 2.6 (b) shows the cylinder-cone shape cavity antenna and Figure 2.6(c) shows the cylinder-cone shape cavity antenna with a deformed ground plane design. From Figure 2.6(a) to Figure 2.6(c), the shape of the antenna is gradually open up, and it gives the electromagnetic wave a smoother transition region from the dielectric loading to the air. For this reason, the wave would have less reflection at the interface between the dielectric material and the air. Therefore, the performance, in term of the operating frequency, Figure 2.6(c) is expected to have wider bandwidth than Figure 2.6(b) than Figure 2.6(a). Same reasoning, the performance of Figure 2.6(c) can be further improved by deforming the ground plane more, even starting from the feed point. However, due to fabrication difficulties regarding the feed point, this will not be included in the design consideration.

In theory, the infinitely large conical antenna can operate at any frequencies. However, in real applications, it always has both high and low frequency limit. In the designs, the low frequency limit is determined by the size of the antenna. When the frequency becomes lower, the wavelength becomes longer, and the electrical size of the antenna becomes very small. For this reason, the antenna would not provide a good smooth region for the wave to go from the transmission line to the air. Thus, most of the wave is reflected back, and it will not radiate. When the frequency becomes higher, the wavelength becomes shorter, and the electrical size of the threes antennas shown in Figure 2.6 become infinitely large. This gives a very large transition region for the wave to go from the transmission line to the air. However, the tip of the feed point is also enlarged with respect to the wave. If this tip is not perfect like a cone shape, it degrades the performance. As a result, the manufacture of the feed point controls the high limit of the frequency band.

The simulation and measurement results in Chapter 3 and 4 validate the behaviors of the antenna discussed here. It proofs that the phenomena are some of the guidelines to manipulate the quasi-planar conical antennas.

CHAPTER 3

SIMULATION, FABRICATION AND MEASUREMENT

3.1 Simulation

Unlike the conventional conical antenna's theory, it is extremely difficult to come out with a mathematical expression for the designed quasi-planar conical antenna due to the adding of the dielectric material. Instead, a numerical simulation is used to find the antenna characteristic such as gain, radiation pattern, and the operating frequency range.

To simulate the dielectric loaded conical antenna, a full wave simulation is carried out. The numerical code is based on the method of moment (MOM) following [31].

The antenna geometry is illustrated in Figure 3.1(a). The whole space is divided into two regions: Region 1 is filled with air; and Region 2 is the dielectric region. Parts of the surface between the two regions are made of metal (depicted by solid lines in Figure 3.1(a)); the other parts are dielectric-air interfaces (dashed lines). Two equivalent problems are established in Figure. 3.1(b) and Figure. 3.1(c), respectively. In Figure 3.1(b), there is air in the whole space; the exterior fields are the same as those in Figure 3.1(a); and the interior fields are zero. In Figure 3.1(c), the whole space is filled with the dielectric material ($\varepsilon_r\varepsilon_0$, μ_0); the interior fields are the same as those in Figure 3.1(a), and the exterior fields are zero. In both equivalent problems, electric currents ($\mathbf{J}_1$ and $\mathbf{J}_2$) and magnetic currents ($\mathbf{M}_1$ and $\mathbf{M}_2$) exist on the surface between the two regions. Since the excitation is at the origin, all the fields and currents have revolutionary symmetry. Then, integral equations can be constructed and numerically solved as detailed in [31].

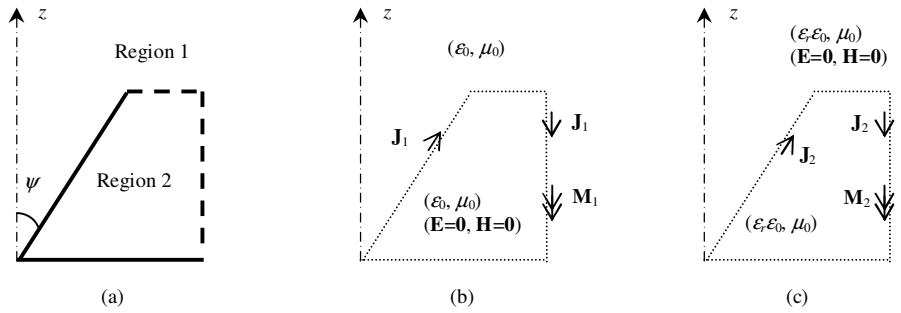

Figure 3.1: Illustration of a revolutionary object with respect to the vertical axis in the middle. (a) antenna geometry, (b) exterior equivalence, and (c) Interior equivalence.

In this antenna configuration, the excitation is in the middle, thus everything is rotationally symmetric (Figure 3.1). That is, $\partial_\phi = 0$.

3.2 Fabrication

To fabrication the designed quasi-planar conical antennas, one challenge is about the material. As discuss previously, the dielectric constant of a material is usually frequency dependent, and if not careful, it will cause the failure to achieve the wide-band performances.

Many materials have been tried to use in the application, however, it is not easy to find a material that has all these characteristics: low dielectric constant, low loss, strong but light, cheap, and easy to cut. In this thesis, a high density polyurethane foam is proposed. The permittivity of this material was measured using HP85070A Dielectric Measurement Probe Kit in conjunction with HP8510 Network Analyzer. The result comes out that the dielectric constant ε_r of the material is roughly between 1.3 and 1.8 for a broad range of frequency. Also, the results shown in Section 4.3 proof the material is indeed low loss. Besides, the material is mechanical strong and stable, light, cheap, and it is easy to cut (compare with metal).

The material can be easily cut into the designed shape using Roland MDX-20 milling machine. However, the method to attach the metal part is critical. Few methods have been tried,

such as using copper tape and copper paint, but they did not work well. The better way is to use thin copper sheets and glue it on to the antenna. When there is a cavity, a complementary shape is built to help the glue process.

Soldering is used to stick the copper to copper, and it requires skills especially on the feed point (as discussed in Chapter 2). Experiments find that when the soldering on the feed tip is not great, the antenna would have a poor performance on the frequencies higher than 10GHz. Pictures below show the fabricated designed antennas.

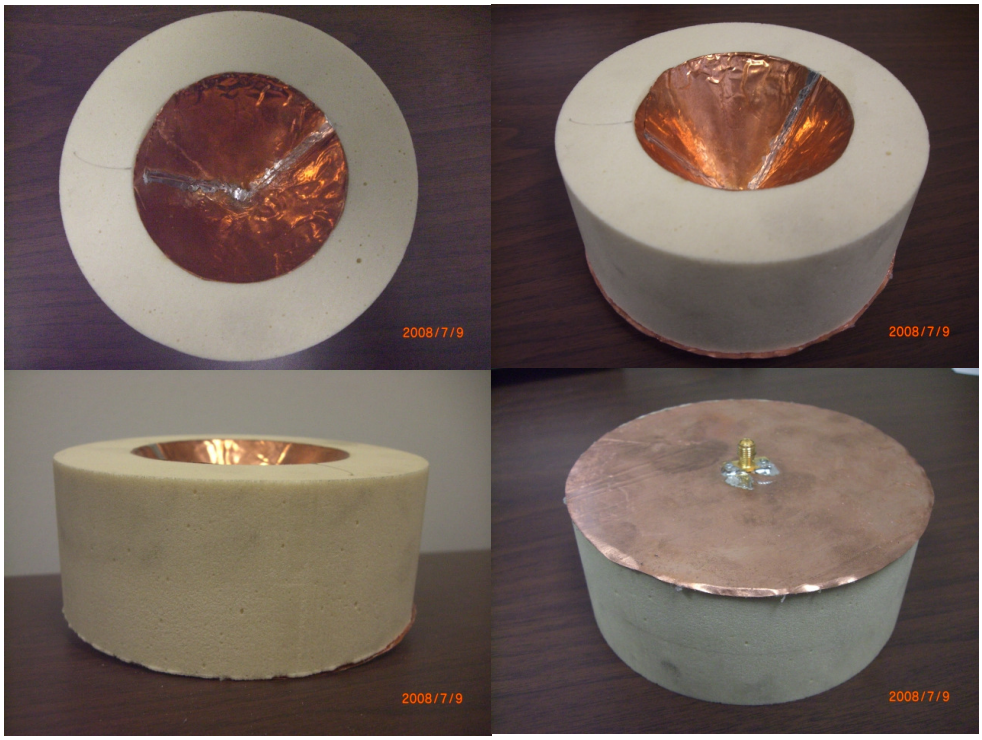

Figure 3.2: Cone shape cavity quasi-planar conical antenna.

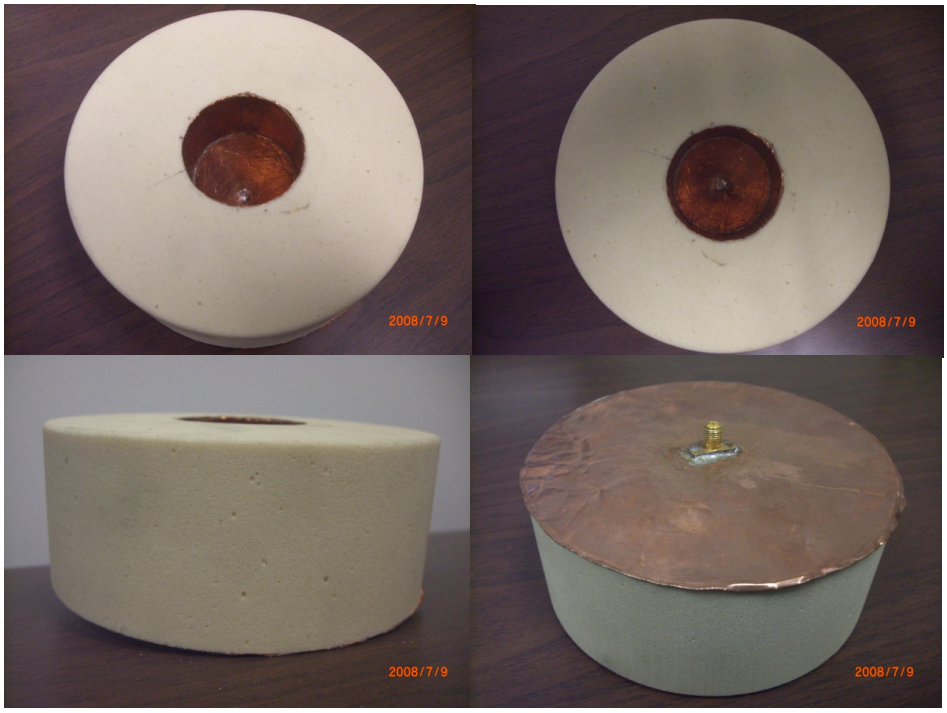

Figure 3.3: Cylinder-cone shape cavity quasi-planar conical antenna.

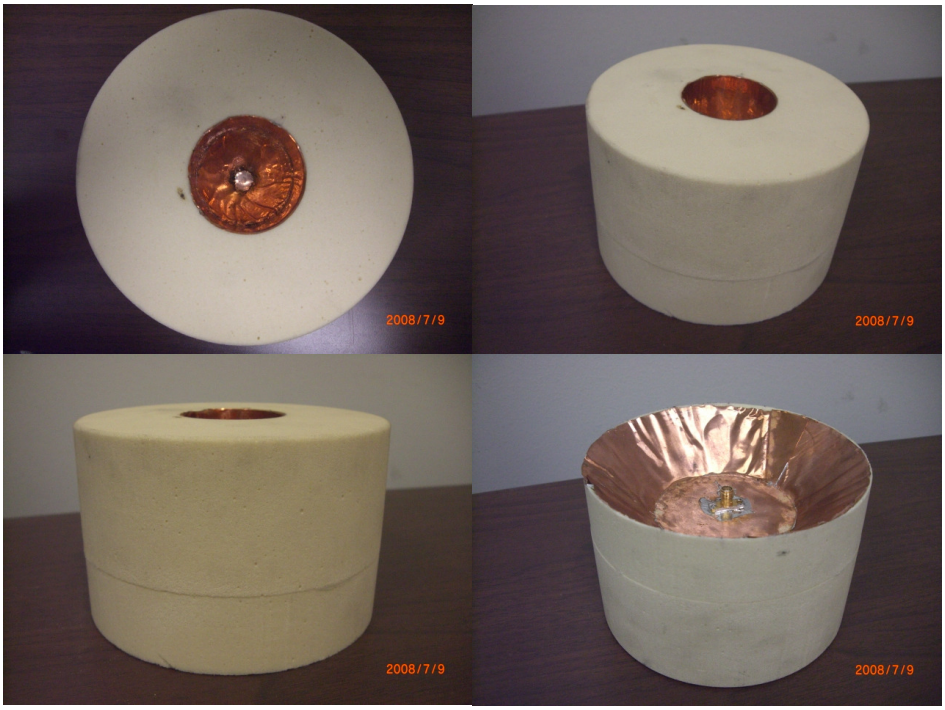

Figure 3.4: Cylinder-cone shape cavity quasi-planar conical antenna with bended ground plane.

3.3 Measurement

To measure the voltage standing wave ratio (VSWR) and the radiation pattern of the antennas, HP8510 Network Analyzer is used.

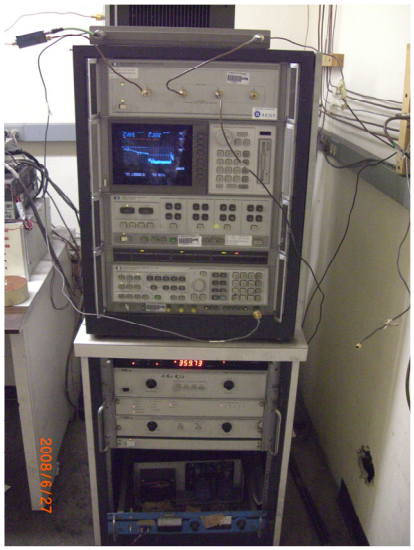

Figure 3.5: HP8510 Network Analyzer

To get the VSWR, first the reflection coefficient Γ is measured by performing a one-port measurement on the AUT (antenna under test). The following equation shows the relationship between the reflection coefficient and VSWR.

$$VSWR = \frac{1+|\Gamma|}{1-|\Gamma|} \tag{3-1}$$

For radiation pattern measurement, a two-port measurement is performed using the network analyzer. First, take a reading from the “through connection”, and find the constant k from the following:

$$P_r = P_t k \tag{3-2}$$

where P_r is the power received, and P_t is the power transmitted. Next, two identical probe antennas are placed face to face with about five meters apart. Follow Equation 3-3 to get the gain of the probe antenna, G_{id} .

$$P_r = \frac{P_t k G_{id}^2 \lambda^2}{(4\pi)^2 R^2} \tag{3-3}$$

where λ is the wavelength and R is the distance between the two antennas. Finally, measure the designed antenna using one of the probe antennas. Then, following the equation to get the gain of the designed antenna, G .

$$P_r = \frac{P_t k G_{id} G \ \lambda^2}{(4\pi)^2 R^2} \tag{3-4}$$

Figure 3.6: Probe antenna used in the measurement (Singer horn antenna model no. A6100).

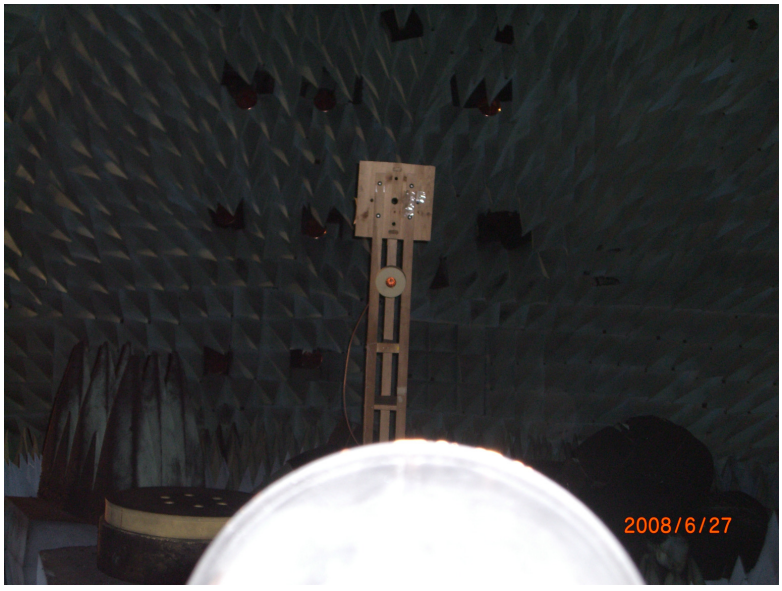

Figure 3.7: Antenna measurement setup.

Figure 3.6 and Figure 3.7 show pictures of the probe antenna and the experiment setup. The AUT is rotated and measured every five degrees for 72 readings. The measurements are from 1GHz to 18GHz.

CHAPTER 4

RESULTS

Following the simulation and measurement procedure, here are the results. The measurement results are pretty well matched with the simulated ones. Also, the performances of the three designed antennas are proofed to be the same as the expected results discussed in Chapter 2.

4.1 Simulated VSWR Results

4.1.1 Simulation Results of cone shape cavity conical antenna

Figure 4.1 shows the dimensions of the designed cone shape cavity quasi-planar conical antenna.

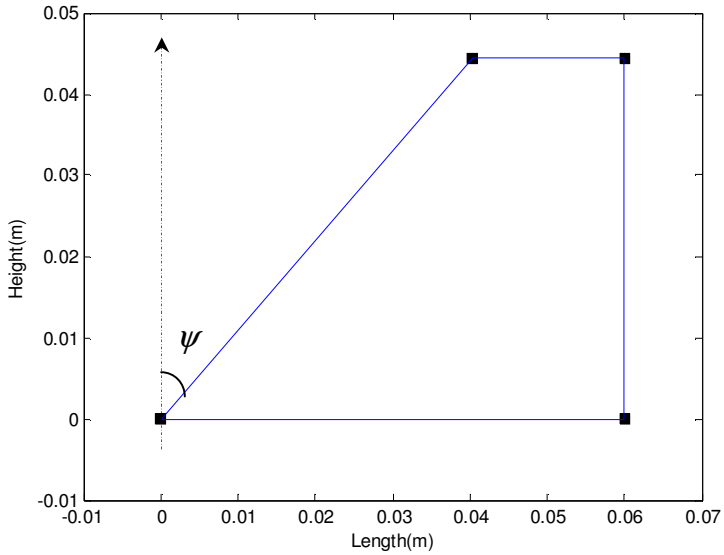

Figure 4.1: Dimensions of the cone shape cavity conical antenna. The geometry has revolutionary symmetric with respect to the length=0 axis. The enclosed area is filled by the material and the outside area is air.

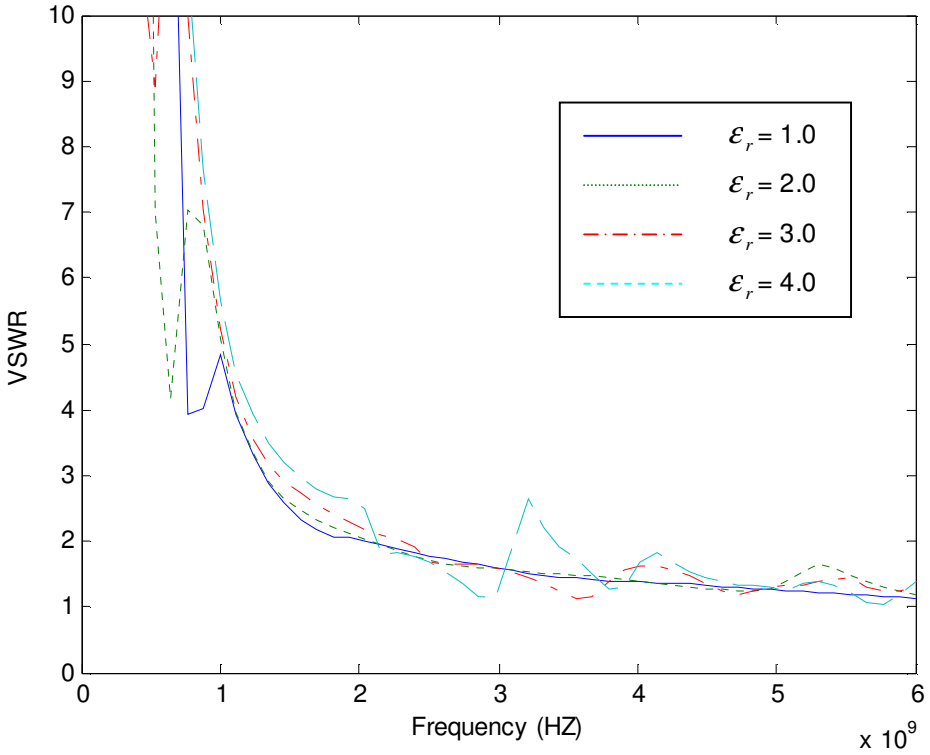

Figure 4.2: VSWR of cone shape cavity conical antenna shown in Figure 4.1.

As discussed in Chapter 2, the input impedance for conical antenna is:

$$Z_{in} = \frac{1}{2\pi}\sqrt{\frac{\mu_0}{\varepsilon_r \varepsilon_0}}\ln\left[\cot\left(\frac{\psi}{2}\right)\right] \qquad (4\text{-}1)$$

where ψ is one-half of the cone angle. For ε_r is increased from 1.0, 2.0, 3.0, to 4.0, the angle ψ also has to change from 47.0, 34.2, 26.6, to 21.4 degrees, respectively, so that the input impedance can remain 50 ohms. Figure 4.2 shows the point that the VSWR value goes below 2 is 1.9GHz, 2.1GHz, 2.3GHz, and 3.4GHz, respectively. It is easy to see that when ε_r is above two, there are some unstable ripples in the higher frequency range. As a reason, the dielectric constant ε_r of the chosen material for this design can not be too high; it is better to stay between 1 and 2. This is another reason that the high density polyurethane foam is a very good

candidate for this design, since its dielectric constant stays roughly between 1.3 and 1.8 for a large band of frequency as discussed earlier in Chapter 3.

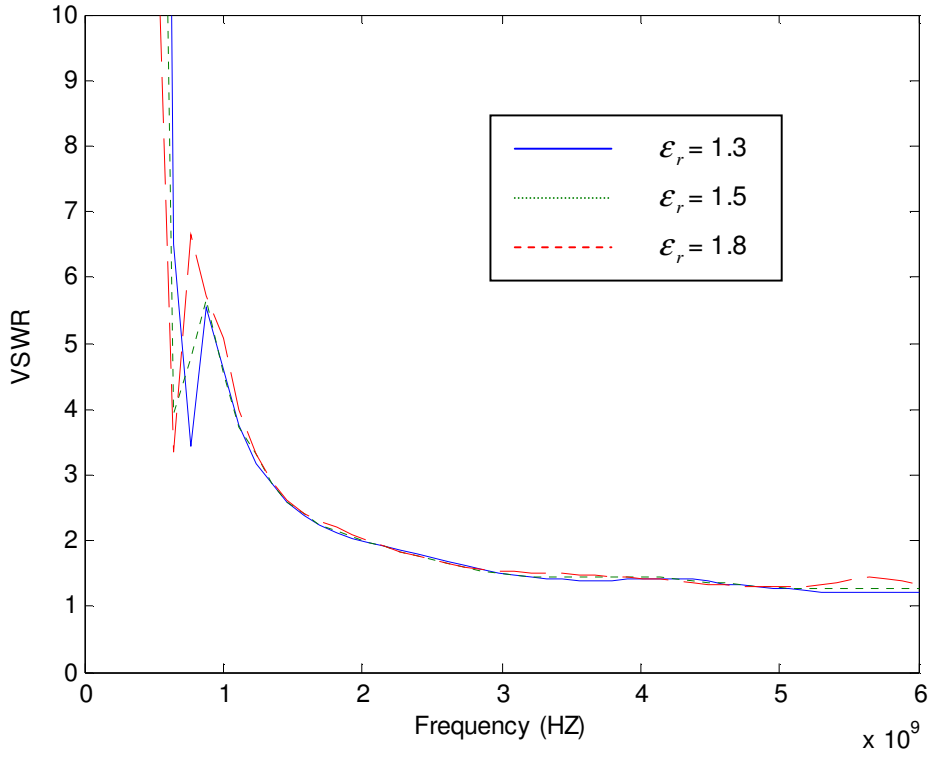

Figure 4.3: VSWR of cone shape cavity conical antenna shown in Figure 4.1 with narrower ε_r range.

Since the dielectric constant of the actual material is from 1.3 to 1.8, let's take a closer look at the simulation results. For ε_r equals to 1.3, 1.5, and 1.8, the angle ψ equals to 42.3, 39.6, and 36.2 degree, respectively, and the VSWR results for these three cases are pretty much the same (shown in Figure 4.3).

However, in reality, the angle ψ has to be a fixed number. Figure 4.4 and 4.5 below show the simulation results when we fix the angle ψ at ε_r=1.3 (42.3 degree) and ε_r=1.8 (36.2 degree) cases, respectively, and sweep the value of ε_r from 1.3 to 1.8.

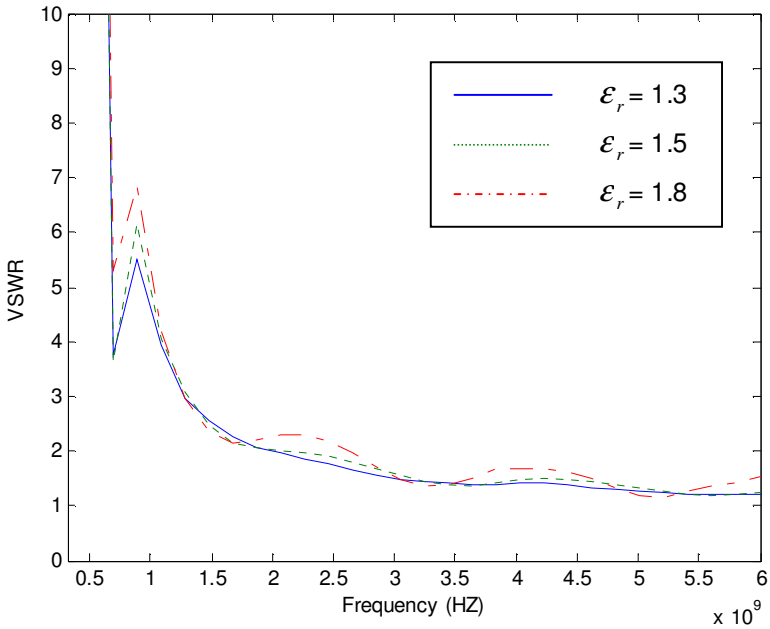

Figure 4.4: VSWR of cone shape cavity conical antenna shown in Figure 4.1 with the half-cone angle fixed at the ε_r=1.3 case (42.3 degree). ε_r is changed from 1.3 to 1.8.

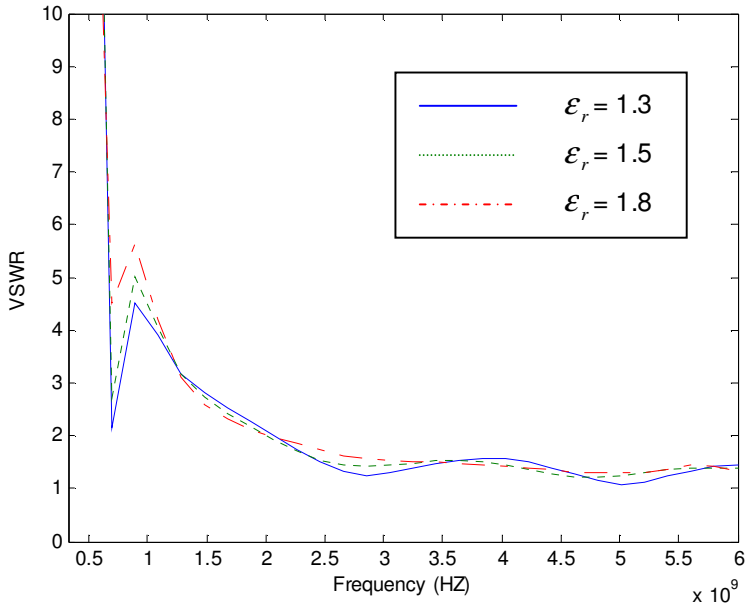

Figure 4.5: VSWR of cone shape cavity conical antenna shown in Figure 4.1 with the half-cone angle fixed at the ε_r=1.8 case (36.2 degree). ε_r is changed from 1.3 to 1.8.

Compare the fixed angle cases with the unfixed angle case in Figure 4.3, the simulations show that it is better to overestimate the angle ψ to the ε_r=1.8 case (36.2 degree). If we compare Figure 4.5 to Figure 4.3, the difference is tolerable.

4.1.2 Simulation Results of cylinder-cone shape cavity conical antenna

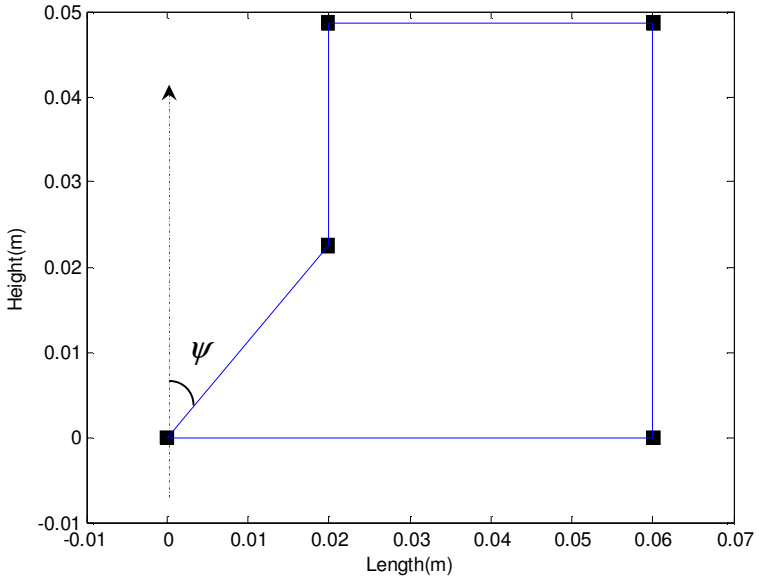

Figure 4.6: Dimensions of the cylinder-cone shape cavity conical antenna. The geometry has revolutionary symmetric with respect to the length=0 axis. The enclosed area is filled by the material and the outside area is air.

Figure 4.7 below shows the simulated VSWR of the conical antenna shape shown in Figure 4.6. The angle ψ varies with respect to ε_r. Same as in the cone shape conical antenna case, when ε_r is 1.3, 1.5, and 1.8, and angle ψ is 42.3, 39.6, and 36.2 degree, respectively. The point that VSWR goes below 2 for the three cases are all very close to 1.5 GHz.

In this design, unlike the cone shape design above, simulations show that when we want to fix the angle, it is better to underestimate the angle ψ to the ε_r=1.3 case (42.3 degree). Figure 4.8 shows the fixed angle case. Compare Figure 4.8 with 4.7, the differences are small.

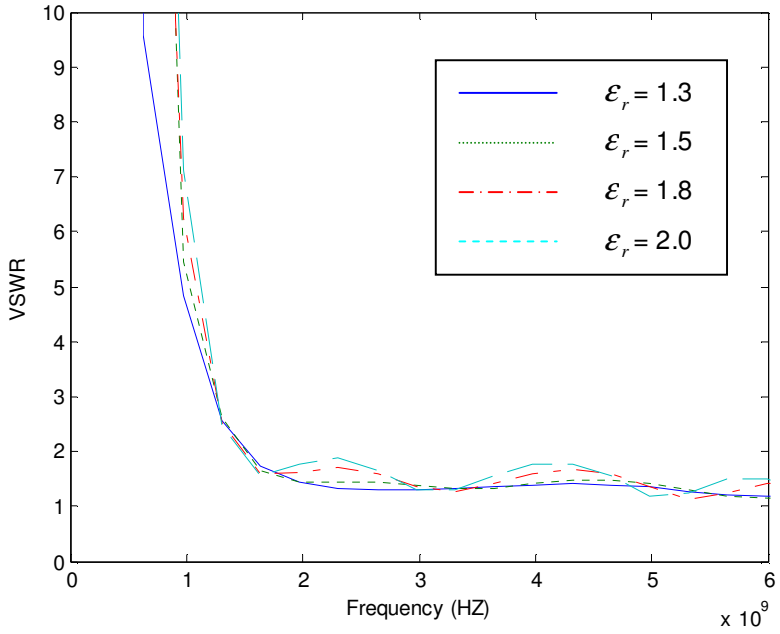

Figure 4.7: VSWR of cylinder-cone shape cavity conical antenna shown in Figure 4.6. ε_r changes from 1.3, 1.5, 1.8, to 2.0, and ψ is 42.3, 39.6, 36.2, and 34.2 degree, respectively.

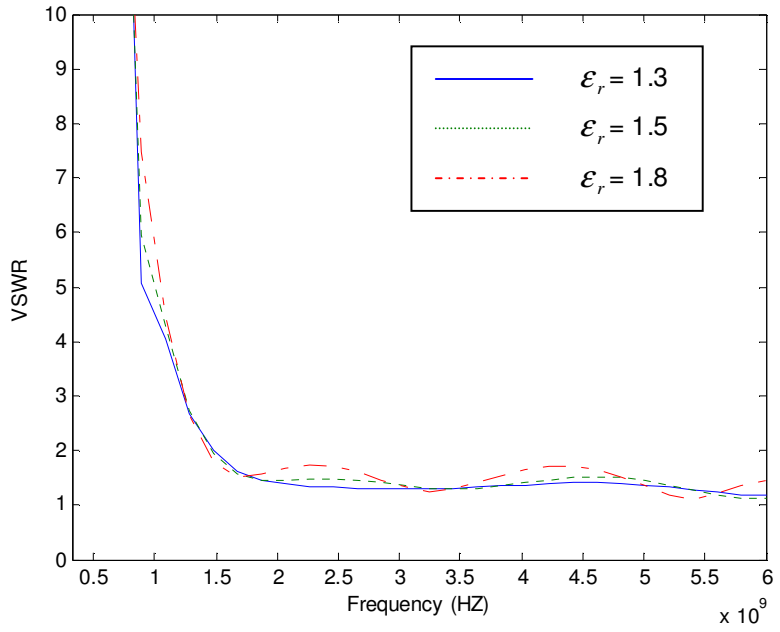

Figure 4.8: VSWR of cylinder-cone shape cavity conical antenna shown in Figure 4.6 with the half-cone angle fixed at the ε_r=1.3 case (42.3 degree). ε_r is changed from 1.3 to 1.8.

4.1.3 Simulation Results of cylinder-cone shape cavity conical antenna with bended ground plane

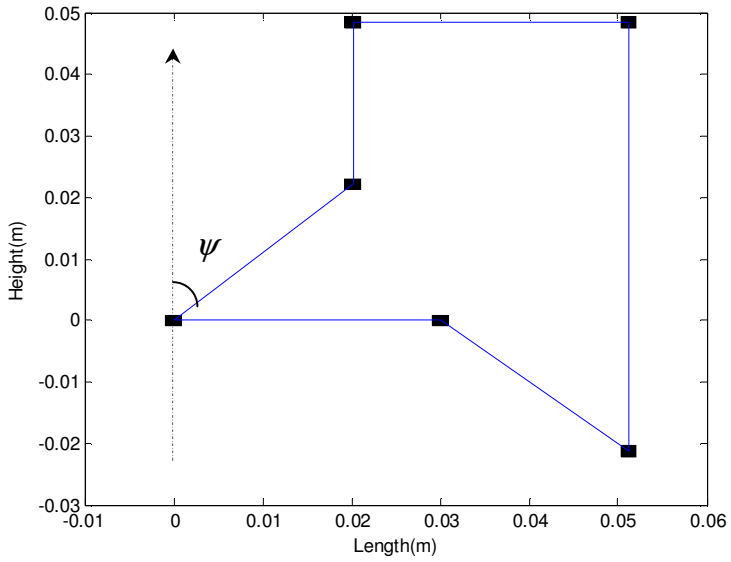

Figure 4.9: Dimensions of the cylinder-cone shape cavity conical antenna with bended ground plane. The geometry has revolutionary symmetric with respect to the length=0 axis. The enclosed area is filled by the material and the outside area is air.

Figure 4.9 shows the configuration of the dipole-like conical antenna design dimensions. To come out with this design, assume the ground plane has a fixed length, and vary the angle that the ground plane is bended downward. That is, if the bended angle is increased, the whole configuration becomes taller and thinner, and vise versa. In this design, the bending angle is 45 degree downward. Simulation shows similar results from about 35 to 55 degree, and 45 is the best. In theory, if the bending degree is larger, the configuration would look more like a dipole. However, in this case, when it bends too much, the configuration becomes too thin, and it affects the result.

Bending point is chosen to be in the middle of the ground plane as shown in Figure 4.6. That is because if it is too close to the feed, the design will be difficult to fabricate; if it is too far away from the feed, the effect of bending ground plane will not be too obvious.

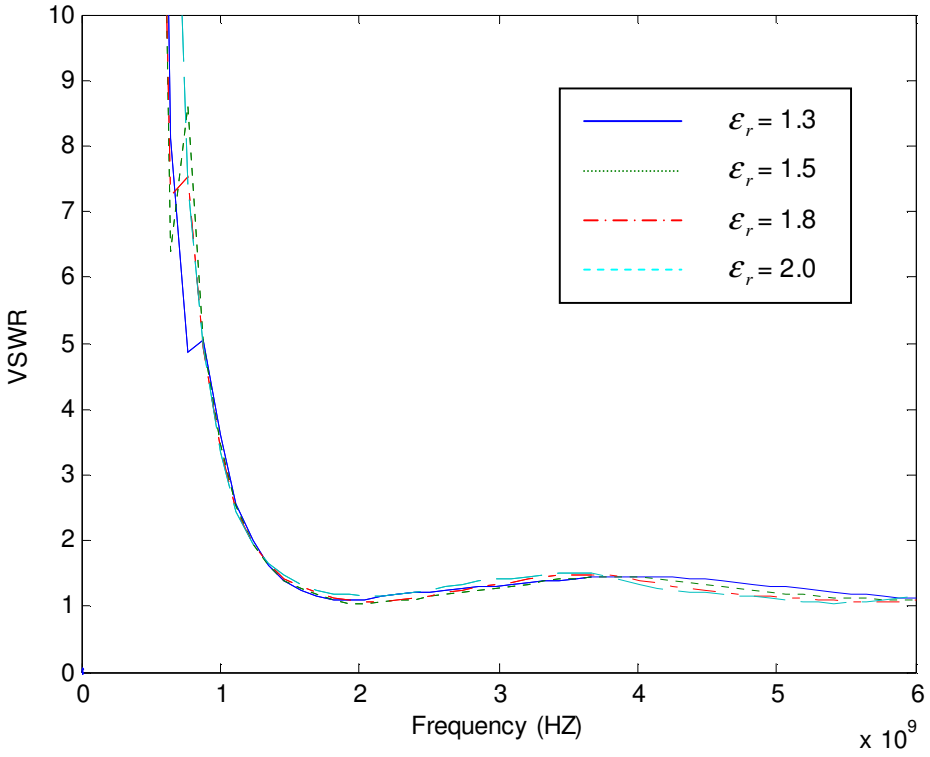

Figure 4.10: VSWR of cylinder-cone shape cavity conical antenna with bended ground plane. shown in Figure 4.9. ε_r changes from 1.3, 1.5, 1.8, to 2.0, and ψ is 42.3, 39.6, 36.2, and 34.2 degree, respectively.

Figure 4.10 shows the VSWR result when the angle ψ varies with respect to the changes of ε_r . The point that the VSWR goes below 2 is about 1.2 GHz for the dielectric constant range between 1.3 and 2.

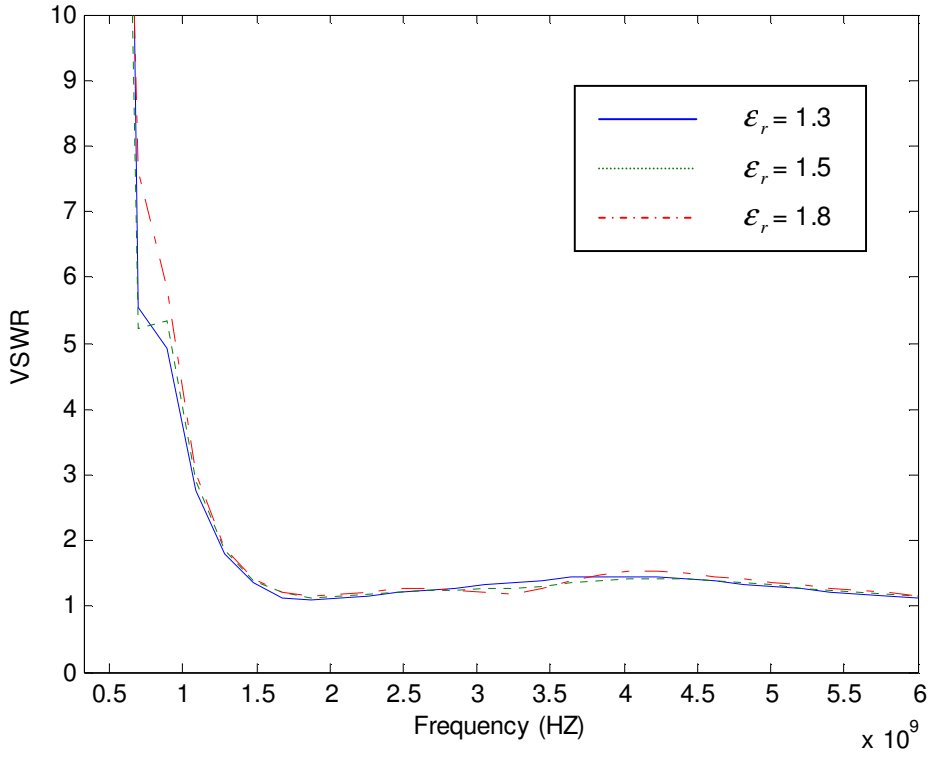

Figure 4.11: VSWR of cylinder-cone shape cavity conical antenna with bended ground plane shown in Figure 4.9 with the half-cone angle fixed at the ε_r =1.3 case (42.3 degree). ε_r is changed from 1.3 to 1.8.

Similar to the cylinder-cone case, in the fixed angle case, it is better to underestimate the angle ψ to the ε_r = 1.3 case (42.3 degree).

Overall, for the three designs, the VSWR results with fixed angles are all very close to the unfixed angle case. These small differences can be tolerable. As a result, even though the dielectric constant is frequency dependent for our material, we can still get the input impedance to be very close to 50 ohms with a fixed cone angle through a wide frequency band. In another word, the designed antenna can be frequency independent although the material is frequency dependent.

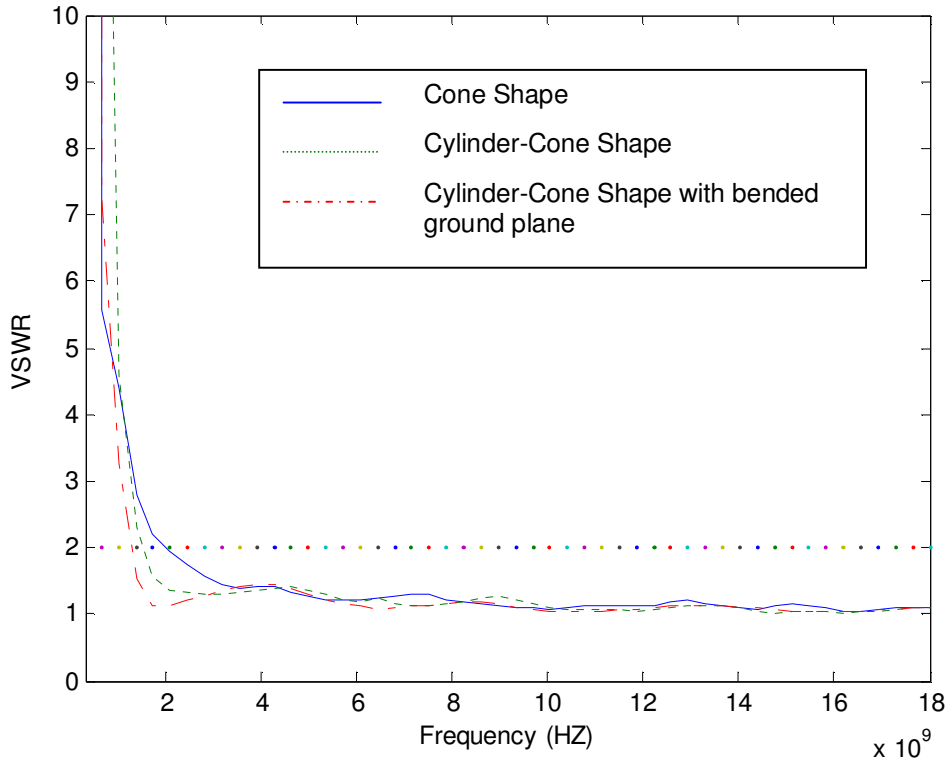

Figure 4.12 Comparison of three types of the designed antenna simulated to 18GHz with ε_r=1.8 for the cone case, and ε_r=1.3 for the other two cases.

Comparing the VSWR of the three antennas, the results in Figure 4.12 show that at frequency greater than 3GHz, they are pretty much similar. The point that the VSWR value goes below 2 for cone shape cavity antenna, cylinder-cone shape and the bended ground plane antenna is 2GHz, 1.5GHz and 1.2GHz, respectively. In another word, the bended ground plane antenna has wider bandwidth than the cylinder-cone shape antenna, and the cylinder-cone shape antenna has wider bandwidth than the cone shape one. At this point, it is easy to see that the simulated results are well matched with the expected results in the design procedure.

4.2 Measured VSWR Results

Following the measuring procedure described in Chapter 3, the measure VSWRs for the three antennas are shown in Figure 4.13-4.15 with simulation values.

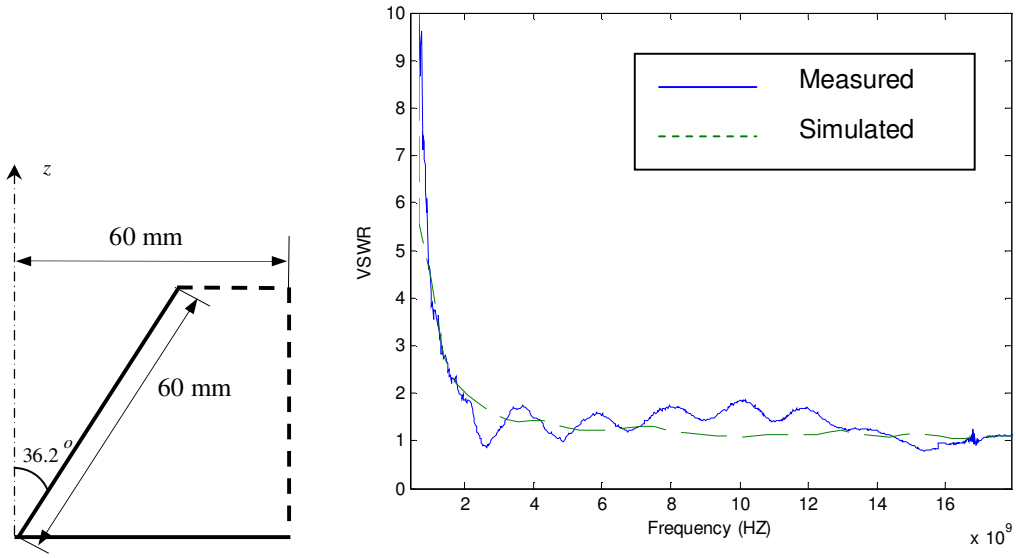

Figure 4.13: Measured VSWR of cone shape cavity conical antenna and comparison with simulated result. The left figure shows the dimensions of the fabricated antenna.

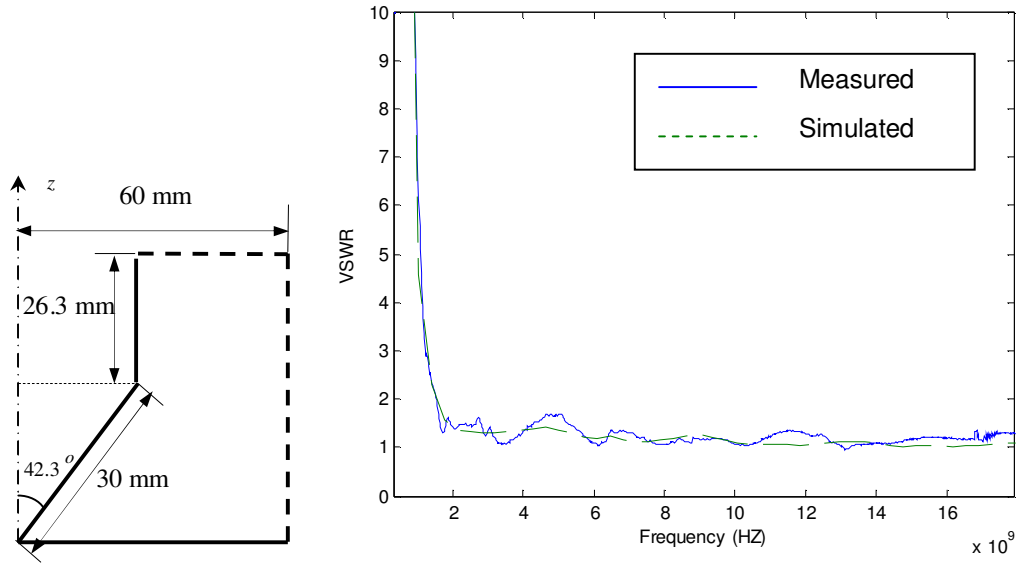

Figure 4.14: Measured VSWR of cylinder-cone shape cavity conical antenna and comparison with simulated result. The left figure shows the dimensions of the fabricated antenna.

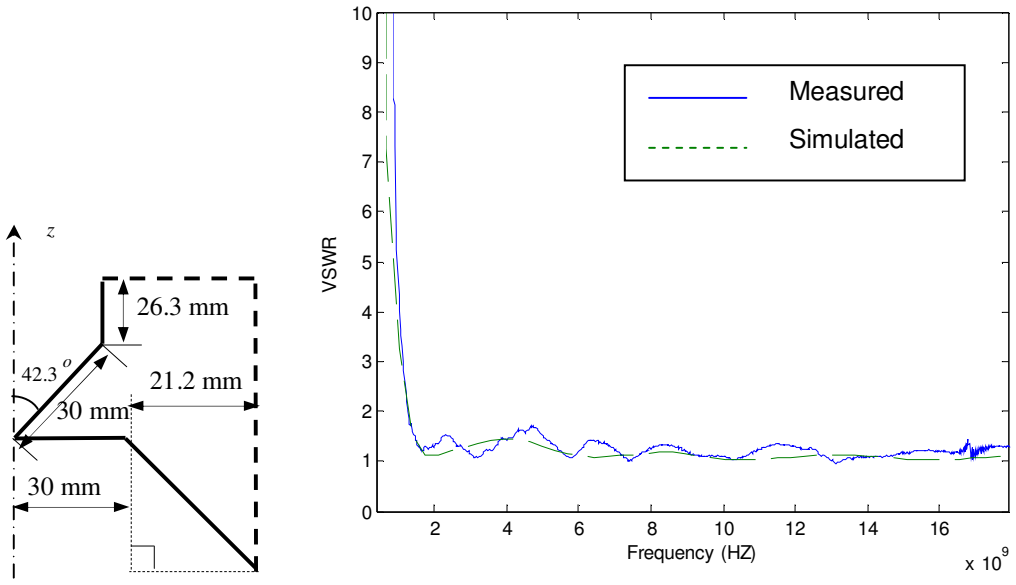

Figure 4.15: Measured VSWR of cylinder-cone shape cavity conical antenna with bended ground plane and comparison with simulated result. The left figure shows the dimensions of the fabricated antenna.

The measured VSWRs are close to the simulation value, but not exactly the same. This could be caused by various reasons, such as the soldering, the glue, the non-perfect cutting, the measuring environment noise, or the measuring system itself. Although it is not perfect, it shows the characteristics we expected. The points that VSWR goes below 2 are all very close to the simulated values, which are 2.0GHz, 1.5GHz, and 1.2GHz, respectively. Also, after that frequency point, the values of the VSWR stay below 2 for the rest of the frequencies, and this is the designed wide-band characteristic.

4.3 Measured and Simulated Radiation Pattern

Following the simulation and measurement procedure described in Chapter 3, here are the radiation patterns for three designed antennas at 2, 5, 8, 11, 14, and 18 GHz.

4.3.1 Radiation Pattern of Cone Shape Cavity Conical Antenna

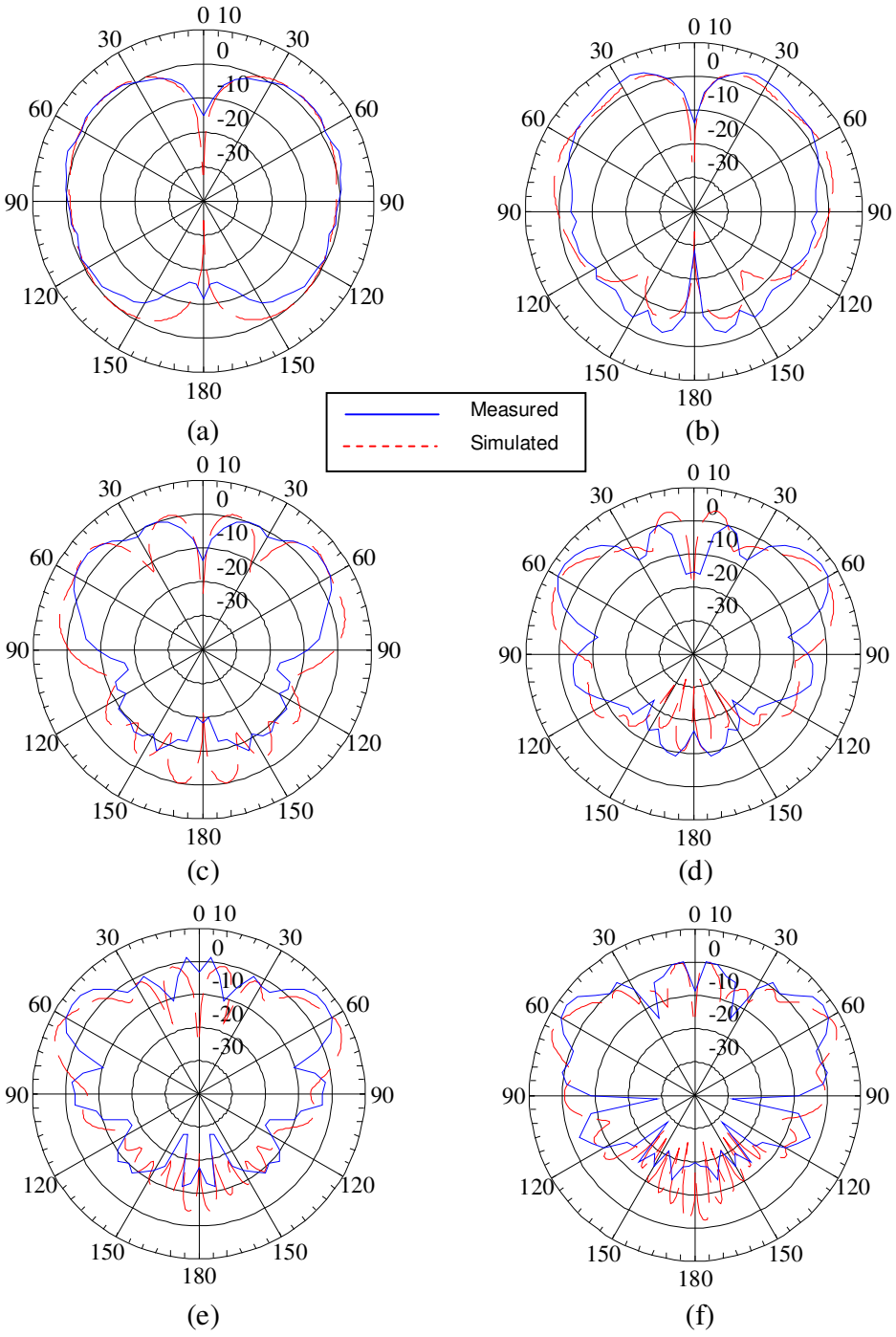

Figure 4.16: Radiation pattern of cone shape cavity conical antenna at (a) 2GHz, (b) 5GHz, (c) 8GHz, (d) 11GHz, (e) 14GHz, and (f) 18GHz. Unit: dBi.

4.3.2 Radiation Pattern of Cylinder-Cone Shape Cavity Conical Antenna

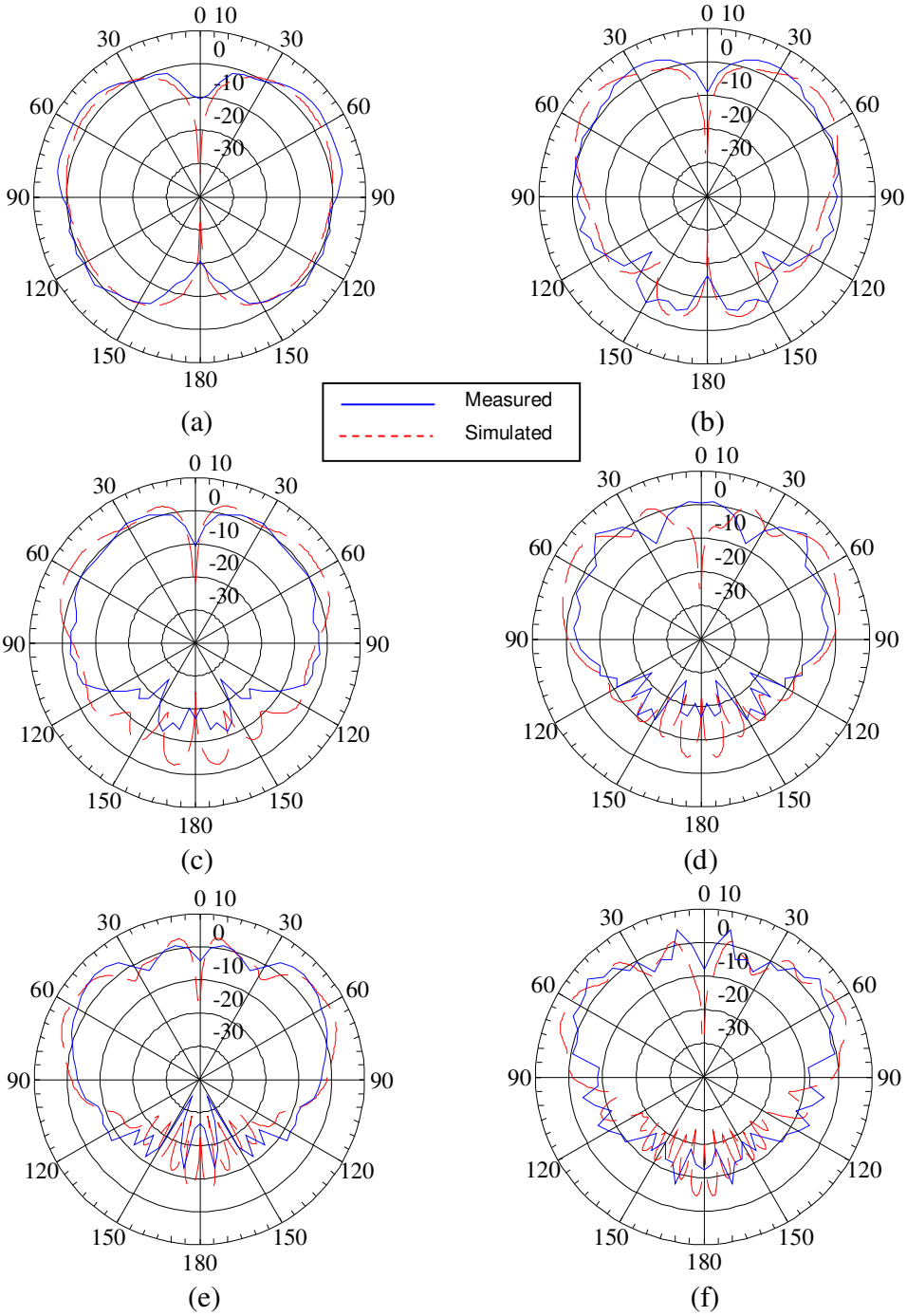

Figure 4.17: Radiation pattern of cylinder-cone shape cavity conical antenna at (a) 2GHz, (b) 5GHz, (c) 8GHz, (d) 11GHz, (e) 14GHz, and (f) 18GHz. Unit: dBi.

4.3.3 Radiation Pattern of Cylinder-Cone Shape Cavity Antenna with Bended Ground Plane

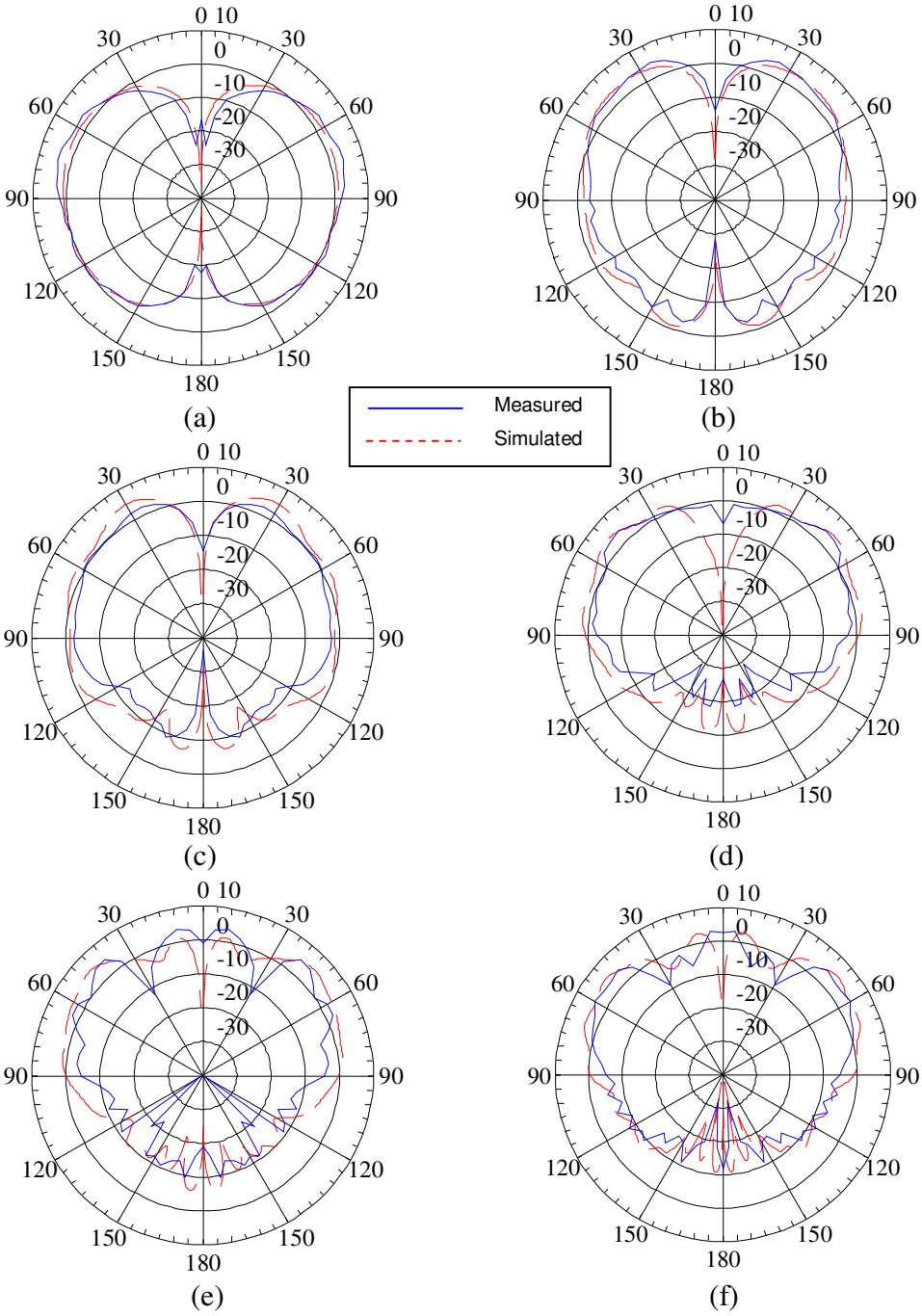

Figure 4.18: Radiation pattern of cylinder-cone shape cavity conical antenna with bended ground plane at (a) 2GHz, (b) 5GHz, (c) 8GHz, (d) 11GHz, (e) 14GHz, and (f) 18GHz. Unit: dBi.

The measured antenna pattern results are all very close to the simulated ones. The maximum gains of the three antennas in different frequencies are all similar; they are all about 5dB. The direction of the maximum gain is about 60 degree for all three antennas, and they all cover a range of elevation.

Overall, the simulated and measured results are well expected. Thus, it can establish a link between the design procedure and the results. In another word, this allows the quasi-planar conical antenna easy to be manipulated. Given a desired frequency range and radiation patter, a quasi-planar conical antenna can be easily built by using the proposed simulation and fabrication methods.

4.4 Effect of Dielectric Material Length

In this section, the ground plane and the dielectric loading are extended to longer length. The cone shape configuration is used.

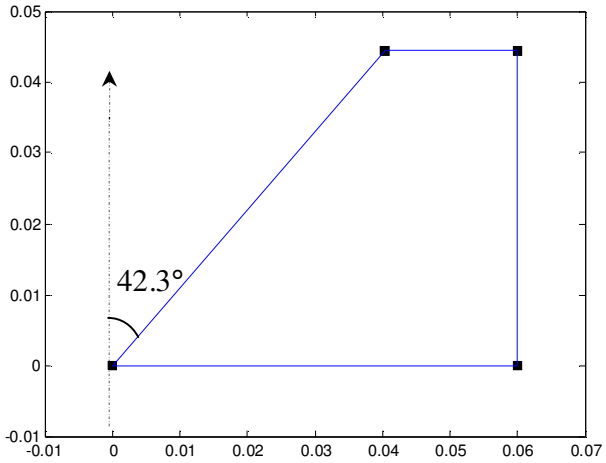

Figure 4.19: Dimensions of the cone shape cavity conical antenna with ground plane length 0.06m. (The geometry has revolutionary symmetric with respect to the length=0 axis. The enclosed area is filled by the material and the outside area is air.)

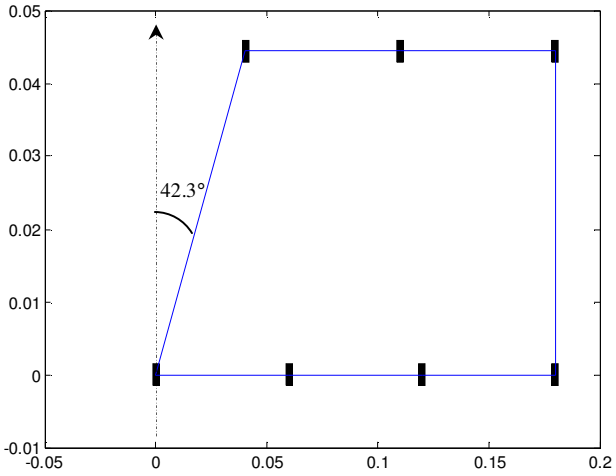

Figure 4.20: Dimensions of the cone shape cavity conical antenna with ground plane length 0.18m. (The geometry has revolutionary symmetric with respect to the length=0 axis. The enclosed area is filled by the material and the outside area is air.)

Figure 4.19 and 4.20 show the cone shape conical antenna with different ground plane shape. In this study, four different length of the ground plane is used: 0.06m, 0.09m, 0.12m, and 0.18m.

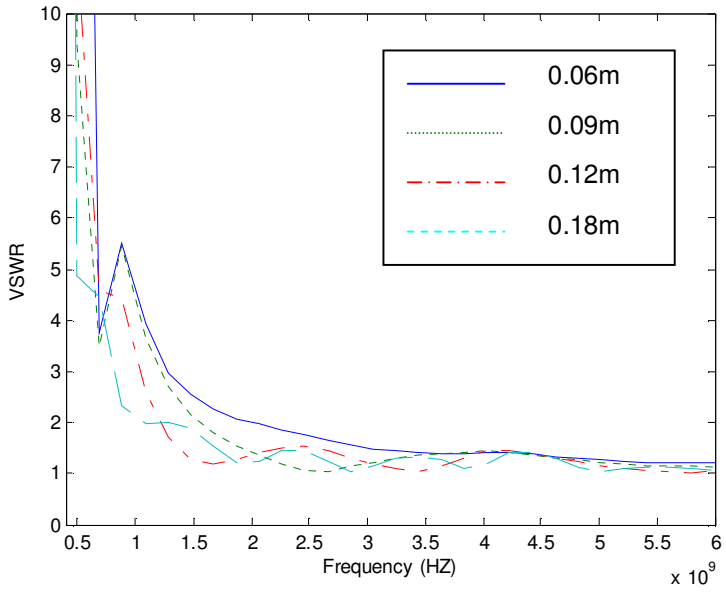

Figure 4.21: Comparison of the VSWR of the four cases up to 6GHz.

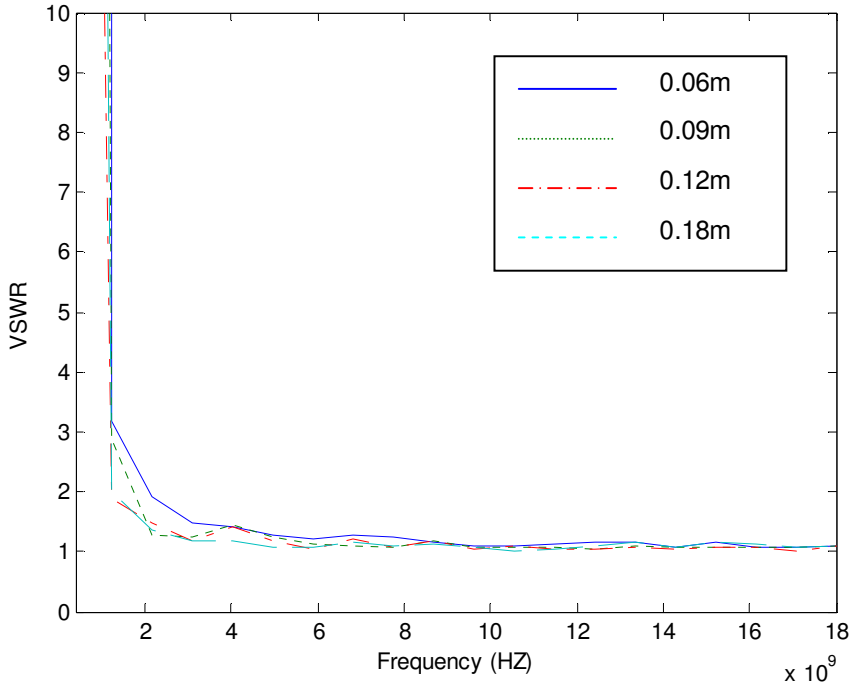

Figure 4.22: Comparison of the VSWR of the four cases up to 18GHz.

Figure 4.21 and 4.22 show the simulated VSWR. As expected, when the ground plane is enlarged, the antenna size becomes larger, and the operate frequency becomes lower. (As it becomes longer, it becomes closer to the infinite sized case, so the frequency band becomes wider).

Pattern measurements are shown below for 2, 5, 8, 11, 14, and 18GHz. It is easy to see that for all four ground plane lengths, the gain of the antenna is pretty much the same (Due to the material is low loss).

When frequency gets higher, the pattern shape has more ripples for the longer ground plane cases. When the frequency gets higher, the interface between dielectric material and air becomes electrically longer, and this cause ripples in the pattern.

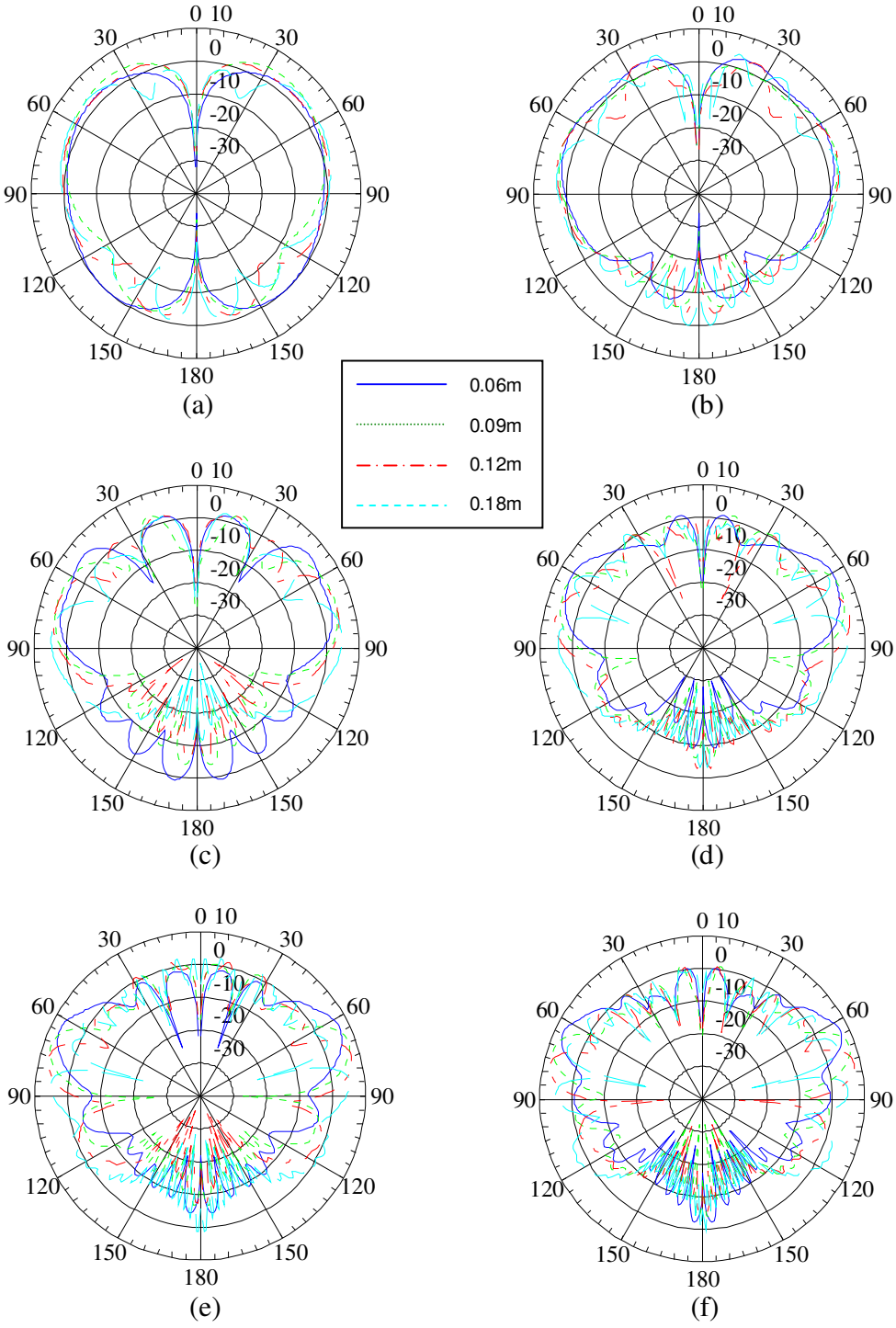

Figure 4.23: Comparison of the radiation pattern for four ground plane lengths at (a) 2GHz, (b) 5GHz, (c) 8GHz, (d) 11GHz, (e) 14GHz, and (f) 18GHz. Unit: dBi.

4.5 Comparison Between Conical and Biconical Antennas

In this section, the performances of the designed cone and cylinder-cone shape cavity conical antennas are compared with the biconical cases. According to the discussion in Chapter 2, the input impedance of a conical antenna is one-half of a biconical antenna. For this reason, to maintain the input impedance at 50 ohms, the cone angle has to be changed.

4.5.1 Cone Shape Conical and Biconical Antenna

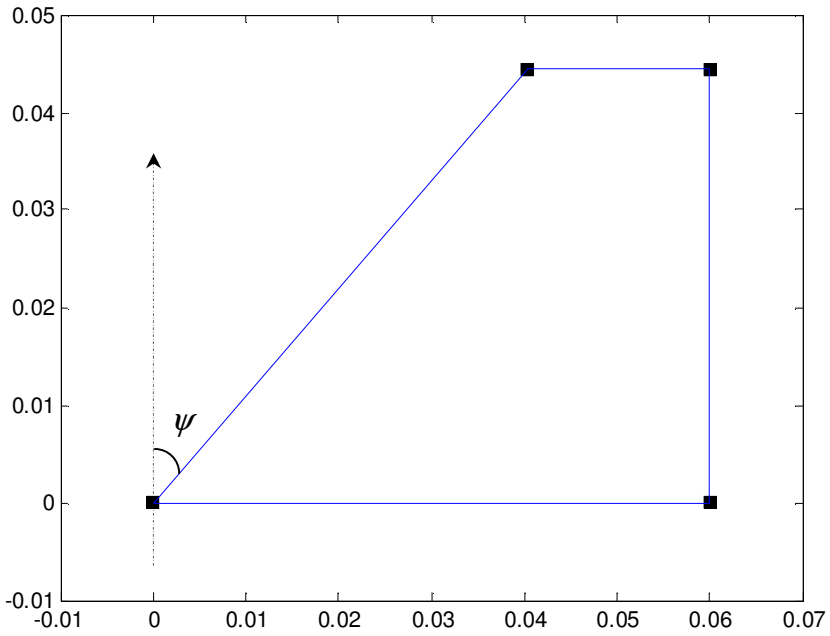

Figure 4.24: Dimensions of the cone shape cavity conical antenna. The half-cone angle ψ is 42.3 degree. (The geometry has revolutionary symmetric with respect to the length=0 axis. The enclosed area is filled by the material and the outside area is air.)

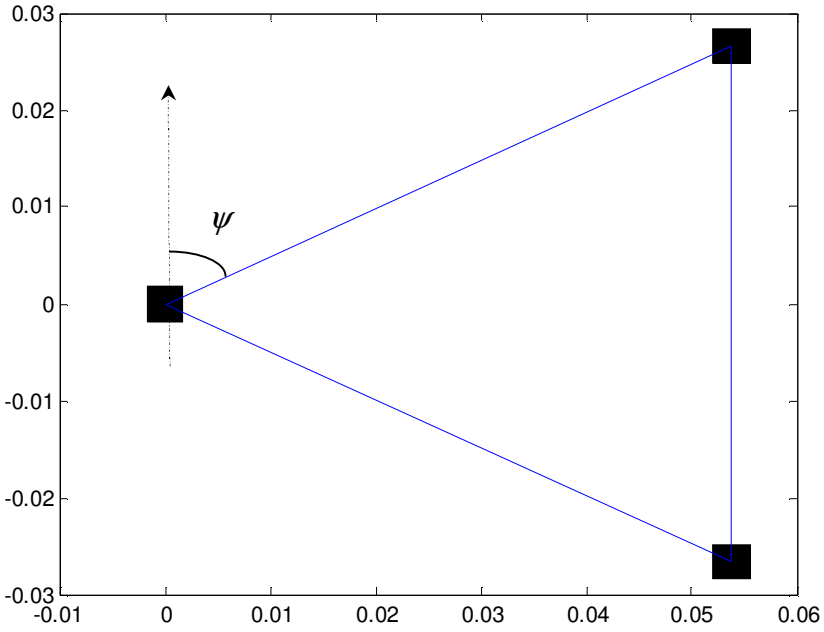

Figure 4.25: Dimensions of the cone shape cavity biconical antenna. The half-cone angle ψ is 63.7 degree. (The geometry has revolutionary symmetric with respect to the length=0 axis. The enclosed area is filled by the material and the outside area is air.)

Figure 4.24 and 4.25 show the cone shape cavity conical antenna and its biconical shape. In this comparison, ε_r = 1.3 is used. As a result, the half-cone angle ψ for the conical case is 42.3 degree. For the biconical case, follow the discussion earlier in Section 2.2, the half-cone angle ψ is calculated to be 63.7 degree to maintain the 50 ohms input impedance. Figure 4.26 below shows the comparison of their simulated VSWR.

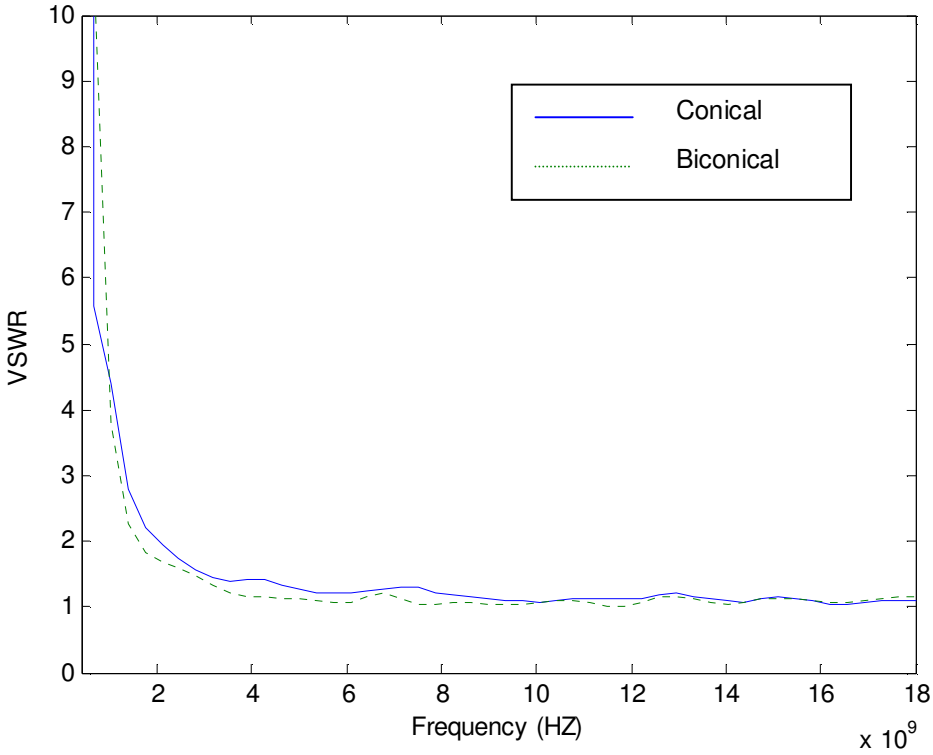

Figure 4.26: Comparison of VSWR of the conical and biconical structure of the cone shape antenna when ε_r =1.3.

The VSWR of the conical and biconical antennas are very similar. The pattern simulations for 2, 5, 8, 11, 14, 18GHz are shown below. As expected, for the biconical case, the maximum gain is always directed to the horizontal direction due to the symmetric. And in the conical case, the maximum gain is always upward (about 60 degrees), because of the ground plane.

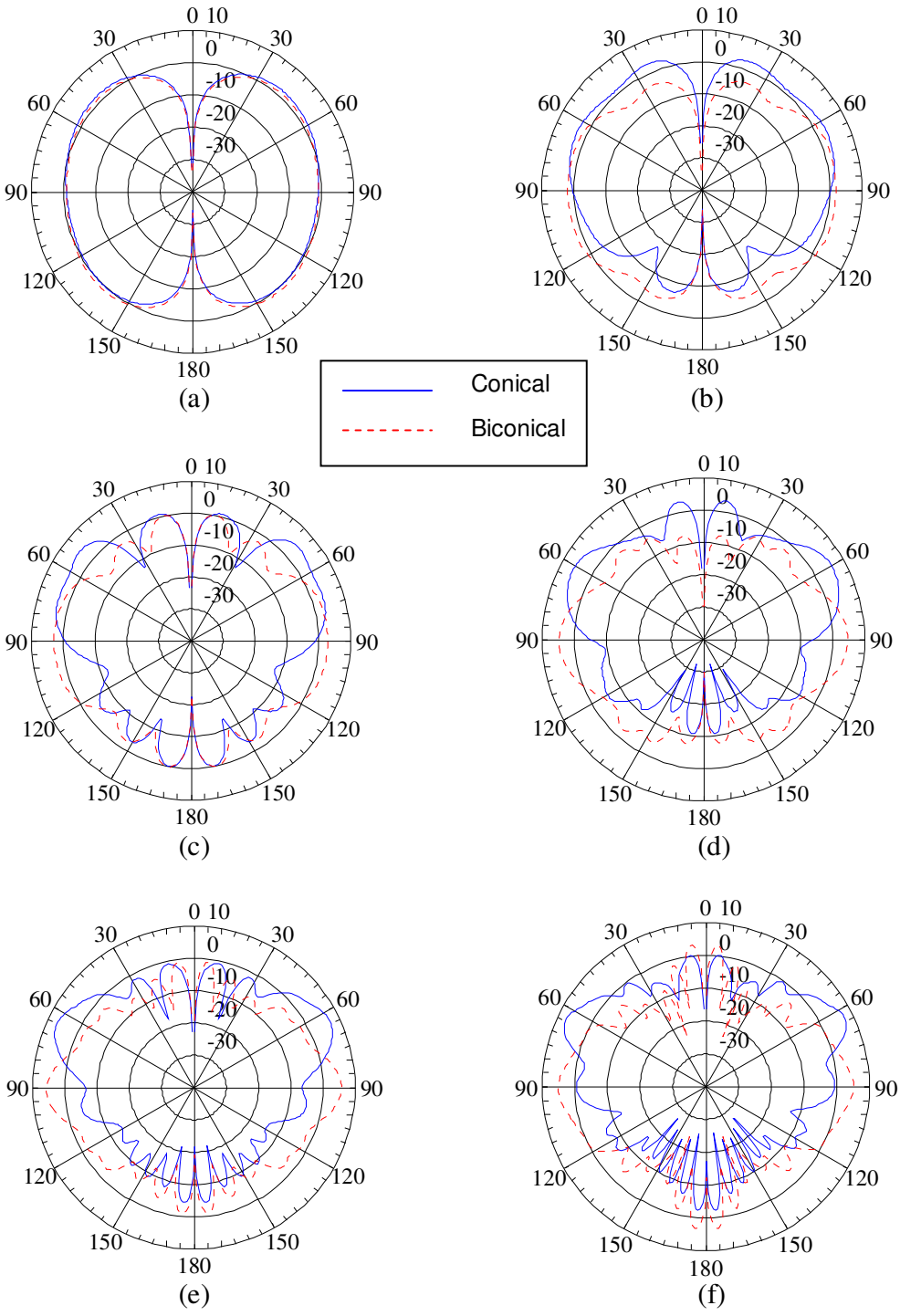

Figure 4.27 Comparison of radiation pattern of the cone shape conical and biconical antennas at (a) 2GHz, (b) 5GHz, (c) 8GHz, (d) 11GHz, (e) 14GHz, and (f) 18GHz. Unit: dBi.

4.5.2 Cylinder-Cone Shape Conical and Biconical Antenna

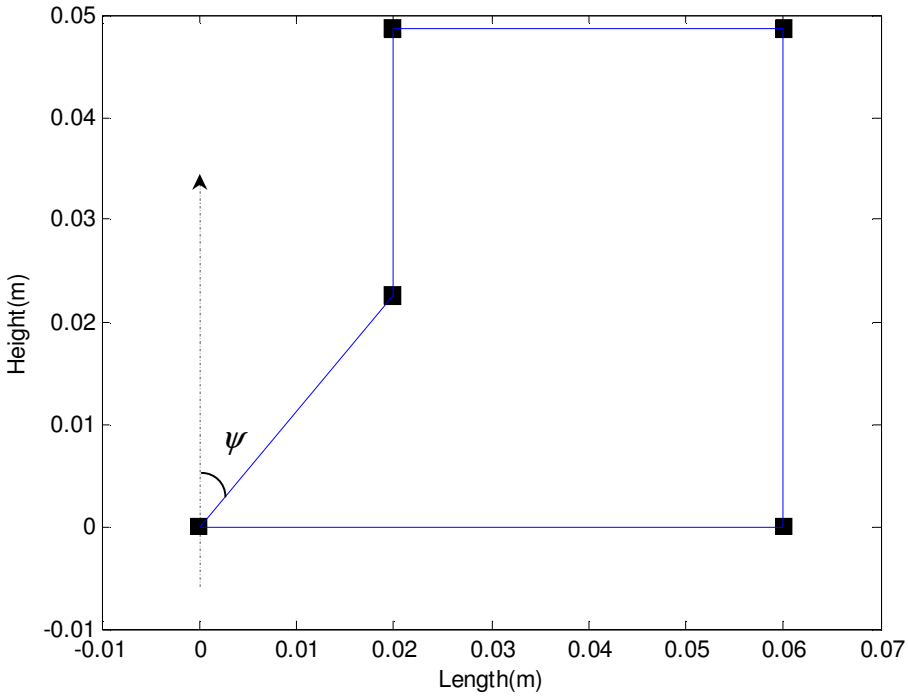

Figure 4.28: Dimensions of the cylinder-cone shape cavity conical antenna. The half-cone angle ψ is 42.3 degree. (The geometry has revolutionary symmetric with respect to the length=0 axis. The enclosed area is filled by the material and the outside area is air.)

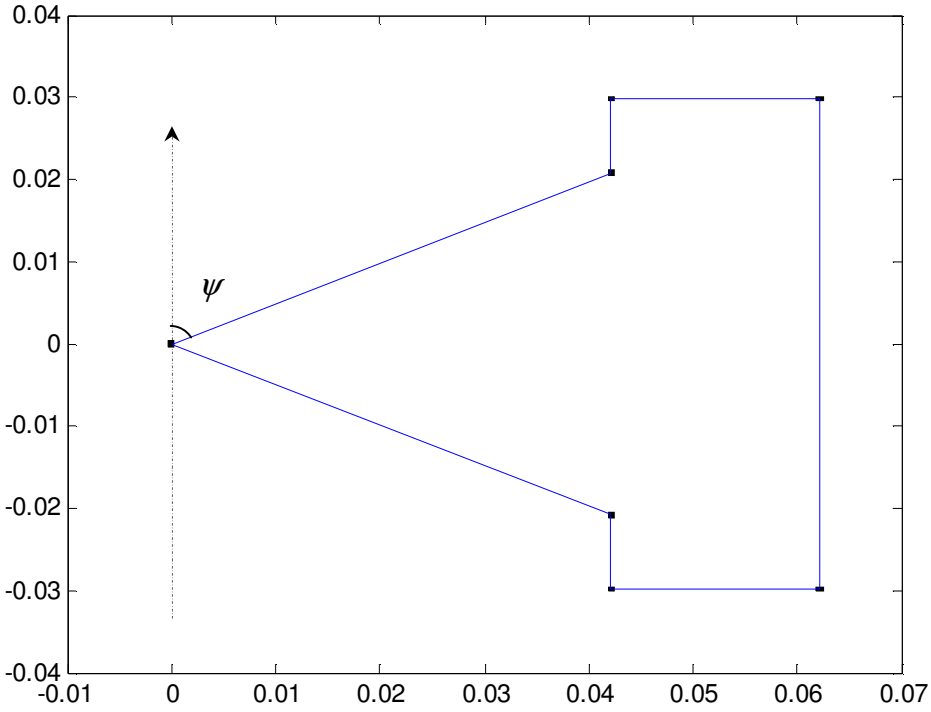

Figure 4.29: Dimensions of the cylinder-cone shape cavity biconical antenna. The half-cone angle ψ is 63.7 degree. (The geometry has revolutionary symmetric with respect to the length=0 axis. The enclosed area is filled by the material and the outside area is air.)

Figure 4.28 and 4.29 show the cylinder-cone shape cavity conical antenna and its biconical shape. Notice that the length of "cylinder part + cone part" remains the same for the two cases. Same as the cone design, since ε_r = 1.3 in this simulation, the angle ψ of the cylinder-cone conical is 42.3 degree and it is found to be 63.7 degree for the cylinder-cone biconical case. Figure 4.30 below shows the comparison of their simulated VSWR.

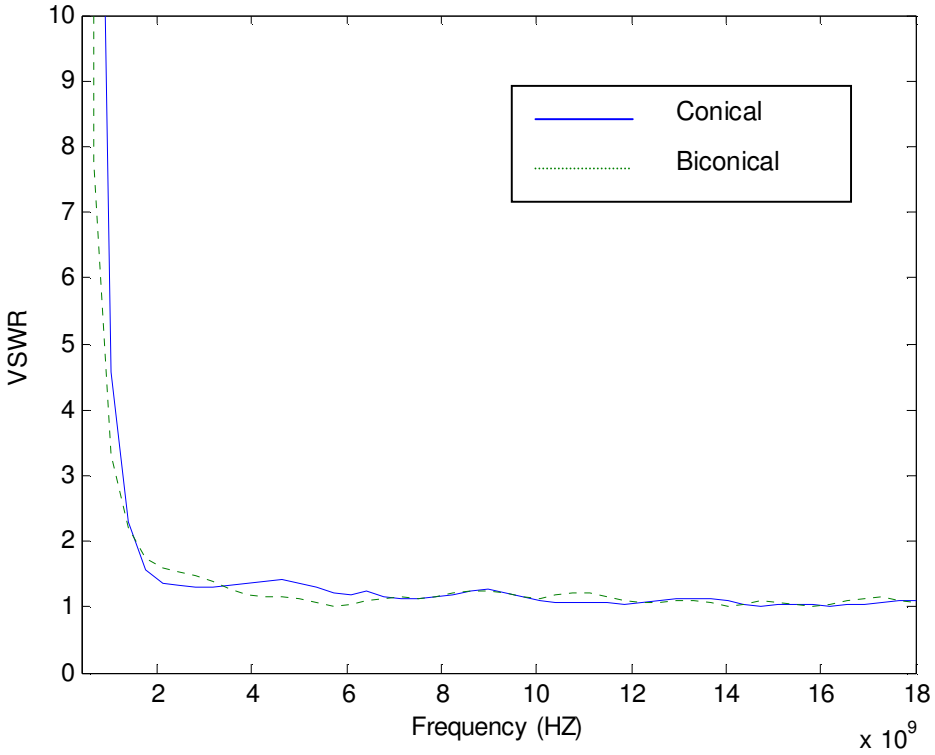

Figure 4.30: Comparison of VSWR of the conical and biconical structure of the cylinder-cone shape antenna when ε_r =1.3.

The VSWR of the conical and biconical antennas are very similar. For both cases, the point where the VSWR goes below 2 is 1.5GHz.

The pattern simulations for 2, 5, 8, 11, 14, 18GHz are shown below. Same as the cone case, for the biconical antenna, the maximum gain is always directed to the horizontal direction, and for the conical antenna, the maximum gain is always upward due to the ground plane.

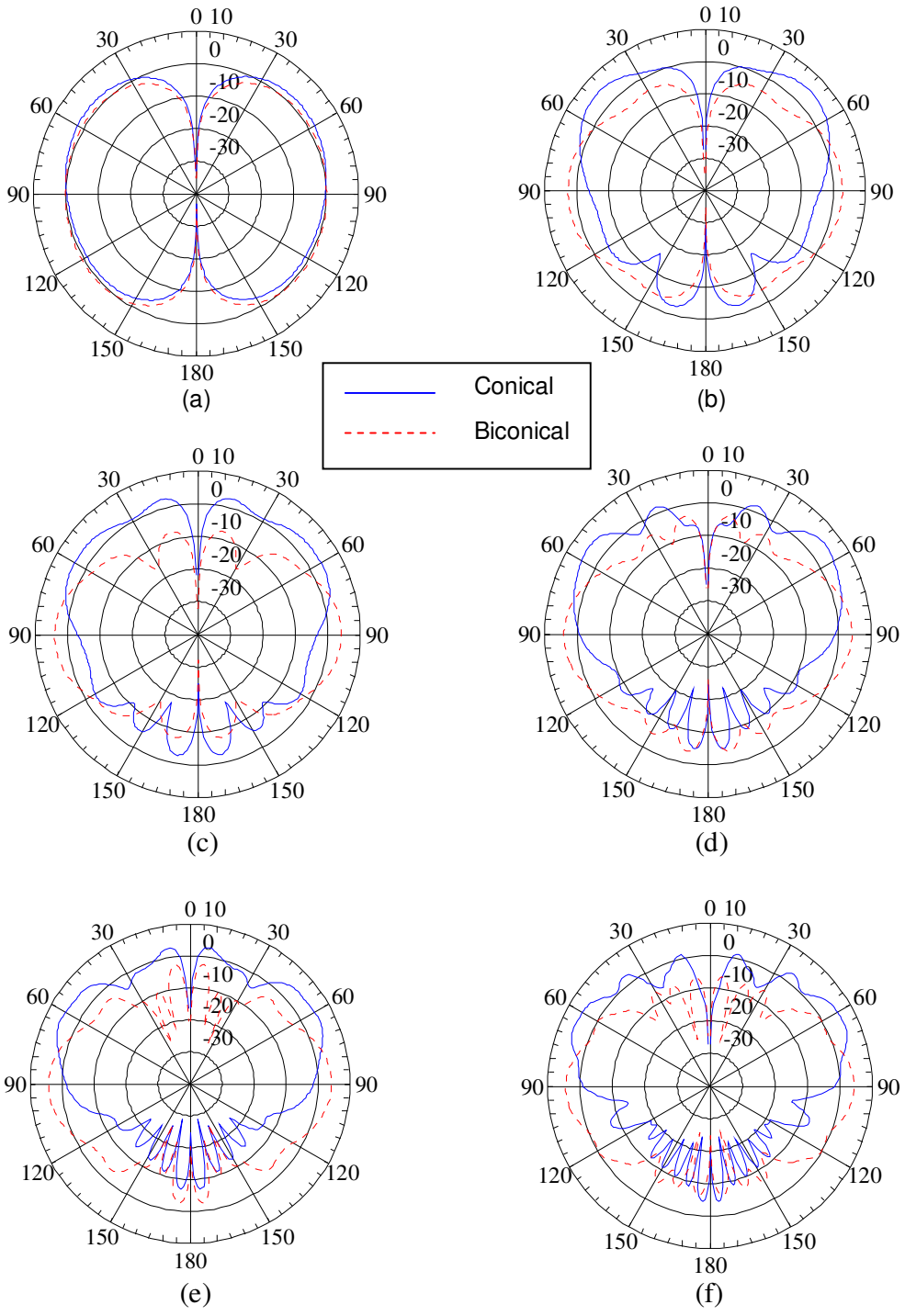

Figure 4.31 Comparison of radiation pattern of the cylinder-cone shape conical and biconical antennas at (a) 2GHz, (b) 5GHz, (c) 8GHz, (d) 11GHz, (e) 14GHz, and (f) 18GHz. Unit: dBi.

CHAPTER 5

SENSOR NETWORK LOCALIZATION

As discussed in Chapter 1, this quasi-planar conical antenna is specially designed for wireless sensor network use. In this Chapter, the designed quasi-planar conical antenna is being tested in a small wireless sensor network. The experiment is divided into two parts. The first one is to test whether the designed antenna could estimate the distance of a given in an accurate manner; the second part is to setup a sensor network and try to locate the given targets.

5.1 Distance Estimation

In this section, the goal is to see whether the designed antenna can measure the distance of a given target accurately. A simple distance measuring method is used.

Figure 5.1 shows the basic setup for the sensor network without any target. The platform is Styrofoam made, and the stand in the middle is used for hold a target since the maximum gain direction for the antenna is about 60 degree upward.

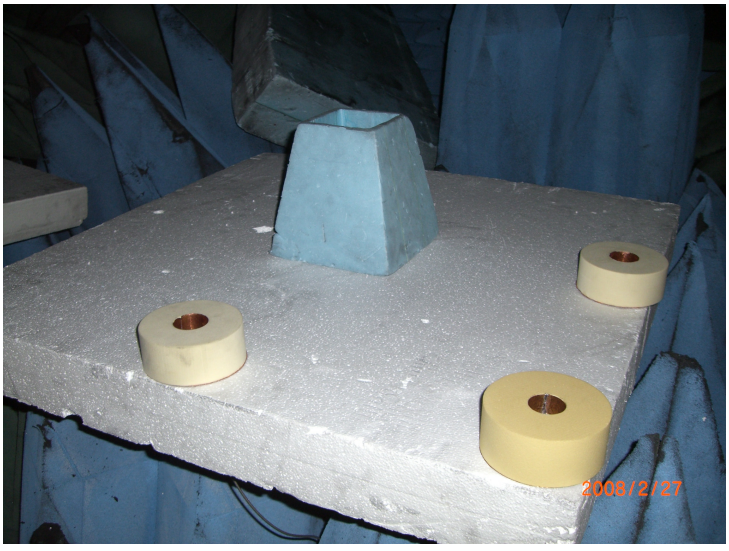

Figure 5.1: Sensor network setup and background measurement.

With the leftmost antenna (Figure 5.1) operating, the time domain signal received is shown below in Fig 5.2.

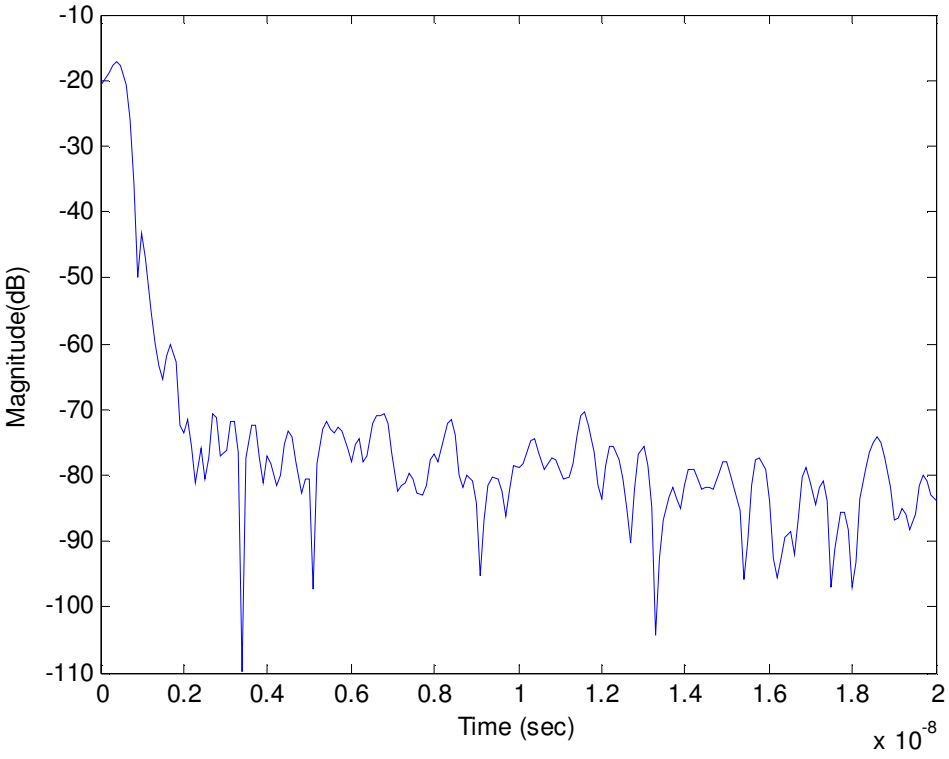

Figure 5.2: Time domain waveform of Figure 5.1 setup (measured by the leftmost antenna).

Having the background information, a metal sphere target is added to the system as shown in Figure 5.3. The distance of the sphere is about 17 inch from the leftmost antenna (measuring directly from the antenna to the surface of the sphere). Figure 5.4 shows the time domain signal received by the left antenna.

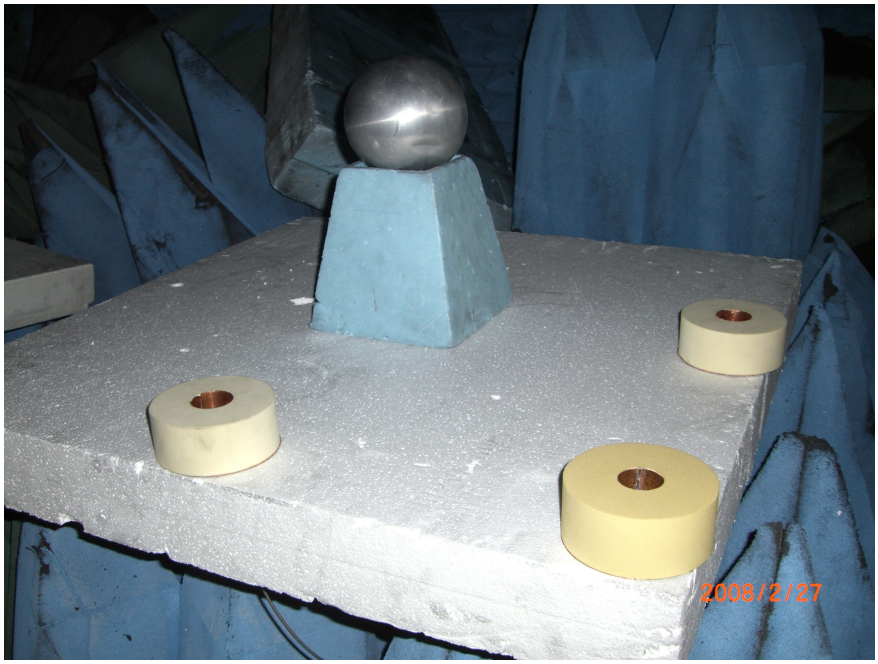

Figure 5.3: Setup with a sphere target (17 inch away from the leftmost antenna).

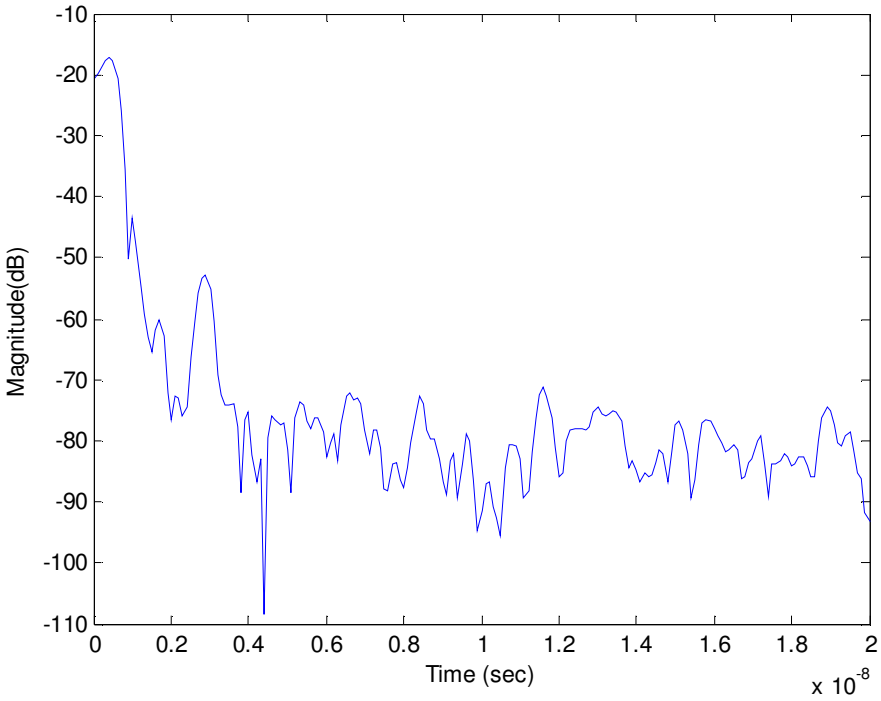

Figure 5.4: Time domain waveform for Figure 5.3 (leftmost antenna).

Compare this signal with the background signal. There is a peak caused by the target. The peak is at 2.866 ns, and this first peak indicates the direct reflection from the target. Base on this, the estimate distance is 16.9252 inches, and it is almost identical to the real distance, 17 inches.

Next, the distance is increased to 21 inches. The result is shown in Figure 5.5.

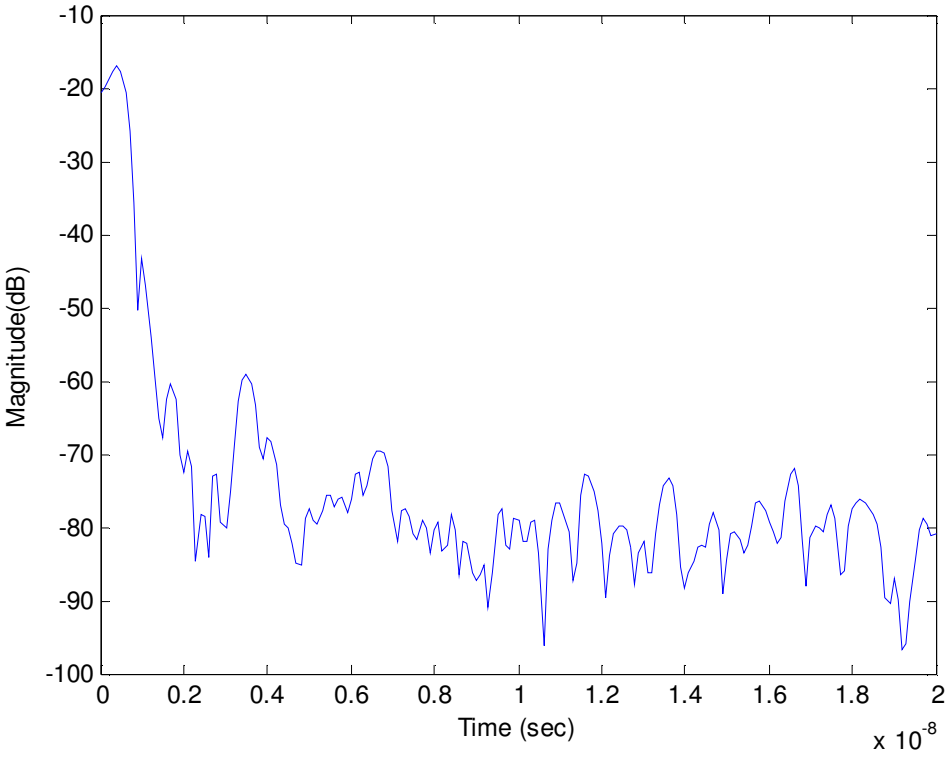

Figure 5.5: Time domain waveform when the target is moved further to 21 inches.

The second peak is at 3.466 ns, and the estimate distance is 20.8685 inch. (Real distance is about 21 inch with respect to the left antenna).

Table 5.1: Relative error of the distance measurements.

	17 Inch Test	**21 Inch Test**
Relative Error	0.44 %	0.63 %

From both results, the estimated distance is very close to the actual distances. Table 5.1 shows the percent error of the distance measurements. From the results, we can claim that the proposed antenna can perform an accurate distance sensing.

However, as the distance increases, the magnitude of the second peak got much smaller. To detect an object further away, we need more power to overcome the noise.

5.2 Localization

Base on above distance estimations, we can setup a sensor network to locate a given object. However, a three-dimensional target localization is too complex due to factors such as targets or sensors at different heights, target size (not a point target), target shapes, etc. This can be itself another study. In this thesis, we assume all the sensors and targets are in the same plane, and follow a two-dimensional localization Minimum Mean Square Estimate (MMSE) algorithm in [32], [33] and [34].

Figure 5.6 shows the sensor network setup with five sensors and three different target locations. Each sensor will get estimated distances from all target locations. Then, combine the results to locate the targets.

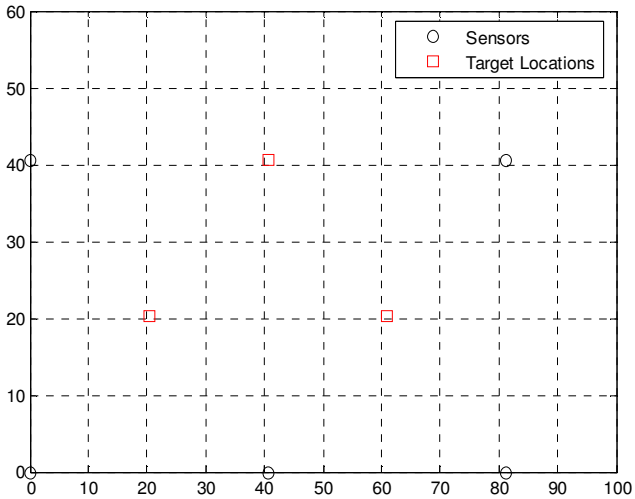

Figure 5.6: Setup for sensor network, the dimension is in centimeters for both axis.

Figure 5.7 to 5.9 below show the results for three target locations. In the figures, the red-circle marks represent the locations of the five sensors. From each sensor there is a circle drawn base on the distance estimated. Then, the cross point for all the circles will be the estimated target location. Compare them to Figure 5.6, the localization results are pretty close to the actual target locations.

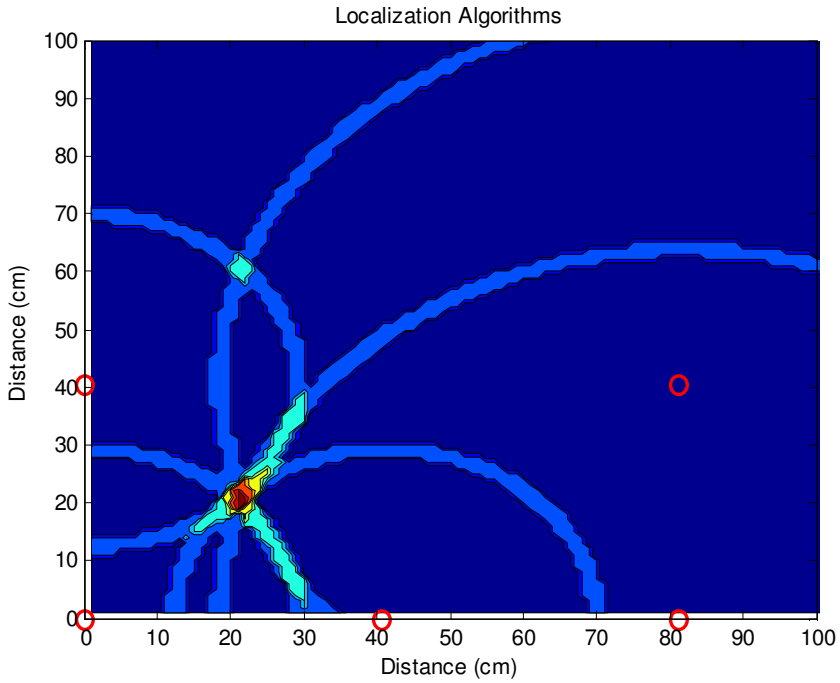

Figure 5.7: Localization results for target location 1.

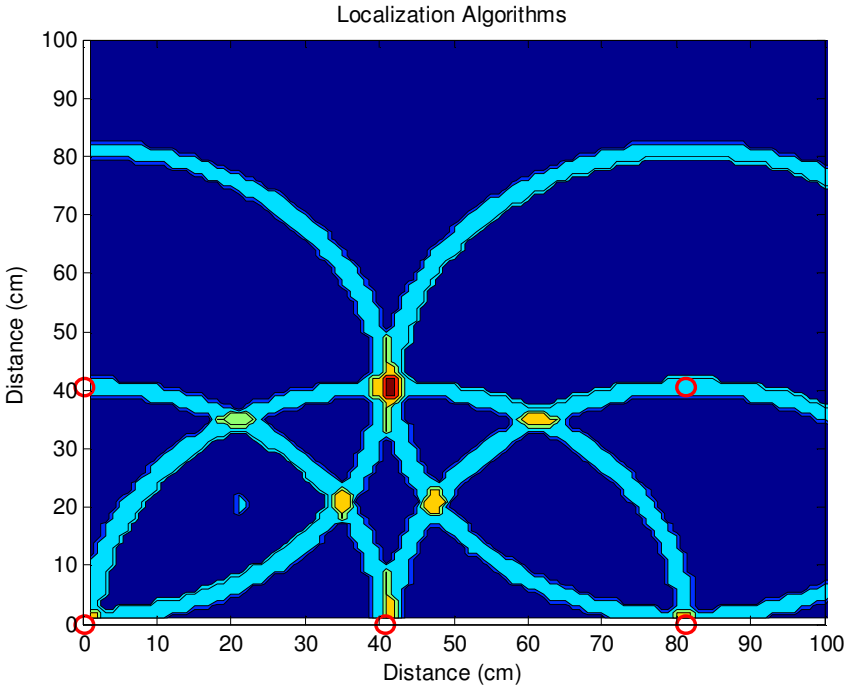

Figure 5.8: Localization results for target location 2.

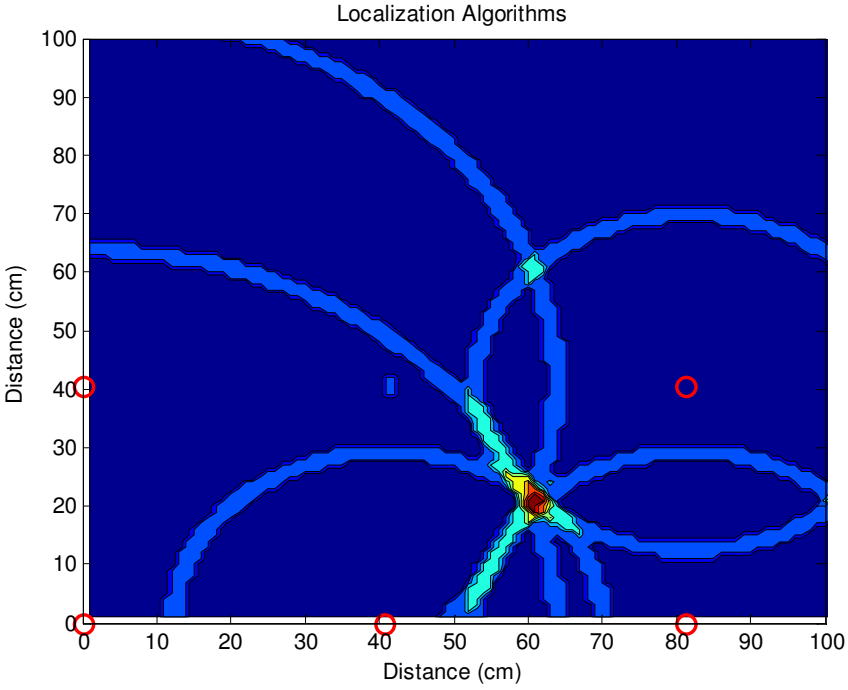

Fig 5.9: Localization results for target location 3.

Overall, this application further shows the usefulness of the designed wide-band omni-directional quasi-planar conical antenna in a wireless sensor network. It is robust and much easier to integrate compared with the conventional conical antenna.

REFERENCES

[1] D. J. Cook and S. K. Das, *To appear in Smart Environments: Technologies, Protocols, and Applications.* John Wiley:New York, 2004.

[2] K. Römer, F. Mattern. "The design space of wireless sensor networks". *IEEE Wireless Communications* 11 (6): 54–61. doi:10.1109/MWC.2004.1368897

[3] M. Ditzel and F. H. Elferink, "Low-power radar for wireless sensor networks," Proceedings of the 3rd European Radar Conference, pp. 139-141, September 2006, Manchester UK.

[4] B. Allen, M. Dohler, E. E. Okon, W. Q. Malik, A. K. Brown, and D. J. Edwards (Eds.), Ultra-Wideband Antennas and Propagation for Communications, Radar and Imaging. London: Wiley, 2006.

[5] H. G. Schantz. "A Beief History of UWB Antennas", *IEEE Aerospace and Electronic Systems Magazine*, v 19, n 4, April, 2004, p 22-26

[6] H. G. Aitken. "Syntony and Spark: The Origins of Radio". Princeton: Princeton University Press, 1985.

[7] O. Lodge, "Electric Telegraphy," U.S. Patent 609,154 (August 16, 1898).

[8] P.S. Carter, "Short Wave Antenna," U.S. Patent 2,175,252 (October 10, 1939).

[9] P.S. Carter, "Wide Band, Short Wave Antenna and Transmission Line System," U.S. Patent 2,181,870 (December 5, 1939).

[10] S.A. Schelkunoff, "Ultra Short Wave Radio System," U.S. Patent 2,235,506 (March 18, 1941).

[11] S. A. Schelkunoff, "Advanced Antenna Theory", (New York: John Wiley and Sons, 1952), p. 160.

[12] M. Katzin, "Electromagnetic Horn Radiator," U.S. Patent 2,398,095 (April 9, 1946).

[13] R.W. Masters, "Antenna," U.S. Patent 2430353 (November 4, 1947).

[14] L.N. Brillouin, “Broad Band Antenna,” U.S. Patent 2,454,766 (November 30, 1948).

[15] G. R. Marié, “Wide Band Slot Antenna,” U.S. Patent 3,031,665 (April 24, 1962).

[16] H. Harmuth, “Frequency Independent Shielded Loop Antenna,” U.S. Patent 4,506,267 (March 19, 1985).

[17] X. Liang and M. C. Y. Wah, “Low-profile broadband omnidirectional monopole antenna,” *Microwave and Optical Technology Letters*, vol. 25, pp. 135-138, 2000.

[18] K. Nagasawa and I. Matsuzuka, “Radiation field of biconical horn antenna with oblique edges”. *IEEE Antennas and Propagation Society*, v 1, 1990, p 527-530.

[19] X. Liang and M. C. Wah, “Low-profile broadband omnidirectional monopole antenna”. *Microwave and Optical Technology Letters*, Vol. 25, No. 2, April 20 2000.

[20] F. Hoshi, S. Sugawara, K. Adachi, and T. Minewaki, “Proposal of small broadband antennas with improved return loss and radiation pattern”. IEEE, p 2425-2428. 2006.

[21] H. Kawakami and G. Sato, “Broad-band characteristics of rotationally symmetric antennas and thin wire constructs,” *IEEE Transactions on Antennas and Propagation*, vol. 35, no. 1, pp. 26-32, Jan. 1987.

[22] C. Ying and Y. P. Zhang, “A planar antenna in LTCC for single-package ultrawide-band radio”. *IEEE Transactions on Antennas and Propagation*, vol 53, no. 9, Sept. 2005.

[23] J. Jung, W. Choi, and J. Choi, "A small wideband microstrip-fed monopole antenna," *IEEE Microwave and Wireless Components Letters*, vol. 15, no. 10, pp. 703-705, October 2005.

[24] G. Zheng, A. A. Kishk, A. W. Glisson, and A. B. Yakovlev, “A broadband printed bow-tie antenna with a simplified balanced feed”. *Microwave and Optical Technology Letters*. vol 47, no. 6, Dec. 2005.

[25] G. Y. Chen and J. S. Sun, “Low profile planar dipole antenna”. *Electronics Letters*. vol 40, no. 13, Jun. 2004.

[26] K. Wong, Y. Chi, C. Su, and F. Chang, “Band-notched ultra-wideband circular-disk monopole antenna with an arc-shaped slot”. *Microwave and Optical Technology Letters*. vol 45, no. 3, May 2005.

[27] N. P. Agrawall, G. Kumar, and K. P. Ray, “Wide-band planar monopole antennas”. *IEEE Transactions on Antennas and Propagation*. vol 46, no. 2, Feb. 1998.

[28] G. B. Gentili, M. Cerretelli, and L. Cecchi, "Coated conical antennas for automotive application," *Journal of Electromagnetic Waves and Applications*, vol. 18, no. 1, pp. 85-97, 2004.

[29] C. A. Balanis, *Antenna Theory: Analysis and Design*. John Wiley & Sons. Jew Jersey. 2005.

[30] R. Plonsey, and R. E. Collin. “Principles and Applications of Electromagnetic Fields “. McGraw-Hill. New York. 1961.

[31] L. N. Medgyesi-Mitschang, J. M. Putnam, and M. B. Gedera, "Generalized method of moments for three-dimensional penetrable scatterers," *Journal of the Optical Society of America A*, vol. 11, no. 4, pp. 1383-1398, 1994.

[32] C. Chang, A. Sahai, "Object tracking in a 2D UWB sensor network," *Asilomar Conference on Signals, Systems, and Computers*, November 2004.

[33] M. Soumekh, *Synthetic Aperture Radar Signal Processing with MATLAB Algorithms*, John Wiley & Sons, Inc. 1999.

[34] K. Trasi, “Localization Algorithms for Passive Targets in Radar Networks”. MS Thesis. University of Texas at Arlington, Arlington, 2007.

BIOGRAPHICAL INFORMATION

Tsungyin Wu received his bachelor degree in the University of Texas at Arlington in electrical engineering, and he is currently working in the wave research center as a master student in electrical engineering in the University of Texas at Arlington.